

Chiral dynamics and partonic structure at large transverse distances

M. Strikman¹ and C. Weiss²

¹*Department of Physics, Pennsylvania State University, University Park, PA 16802, USA*

²*Theory Center, Jefferson Lab, Newport News, VA 23606, USA*

We study large-distance contributions to the nucleon's parton densities in the transverse coordinate (impact parameter) representation based on generalized parton distributions (GPDs). Chiral dynamics generates a distinct component of the partonic structure, located at momentum fractions $x \lesssim M_\pi/M_N$ and transverse distances $b \sim 1/M_\pi$. We calculate this component using phenomenological pion exchange with a physical lower limit in b (the transverse “core” radius estimated from the nucleon's axial form factor, $R_{\text{core}} = 0.55$ fm) and demonstrate its universal character. This formulation preserves the basic picture of the “pion cloud” model of the nucleon's sea quark distributions, while restricting its application to the region actually governed by chiral dynamics. It is found that (a) the large-distance component accounts for only $\sim 1/3$ of the measured antiquark flavor asymmetry $\bar{d} - \bar{u}$ at $x \sim 0.1$; (b) the strange sea quarks, s and \bar{s} , are significantly more localized than the light antiquark sea; (c) the nucleon's singlet quark size for $x < 0.1$ is larger than its gluonic size, $\langle b^2 \rangle_{q+\bar{q}} > \langle b^2 \rangle_g$, as suggested by the t -slopes of deeply-virtual Compton scattering and exclusive J/ψ production measured at HERA and FNAL. We show that our approach reproduces the general N_c -scaling of parton densities in QCD, thanks to the degeneracy of N and Δ intermediate states in the large- N_c limit. We also comment on the role of pionic configurations at large longitudinal distances and the limits of their applicability at small x .

PACS numbers: 13.60.Hb, 12.39.Fe, 14.20.Dh, 11.15.Pg

Contents		
I. Introduction	1	B. Chiral corrections to pion structure 19
II. Chiral dynamics and partonic structure	4	C. Chiral dynamics at large longitudinal distances 19
A. Parametric region of chiral component	4	VIII. Summary and outlook 20
B. Pion distribution in the nucleon	5	Acknowledgments 21
C. Large- b asymptotics	6	References 21
D. Contribution to nucleon parton densities	7	A. Meson-baryon couplings from $SU(3)$ symmetry 23
III. Pion cloud model in impact parameter representation	8	B. Evaluation of coordinate-space distributions 24
A. Modeling finite-size effects	8	
B. Universality at large b	9	
C. Effective pion momentum distribution	10	
D. Extension to $SU(3)$ flavor	11	
IV. Large-distance component of the nucleon sea	11	
A. Isovector sea $\bar{d} - \bar{u}$	11	
B. Isoscalar sea $\bar{u} + \bar{d}$	12	
C. Strange sea s, \bar{s}	13	
D. Flavor asymmetry $\bar{u} + \bar{d} - 2\bar{s}$	14	
V. Transverse size of nucleon	15	
A. Transverse size and GPDs	15	
B. Transverse size from hard exclusive processes	15	
C. Chiral contribution	16	
VI. Pion cloud and large-N_c QCD	17	
VII. Small x-regime and longitudinal distances	18	
A. Growth of core size through diffusion	18	

I. INTRODUCTION

Parton densities summarize the structure of the nucleon probed in high-momentum transfer processes such as deep-inelastic lepton-nucleon scattering and production of high-mass systems (jets, heavy particles) in nucleon-nucleon collisions. They are defined in the context of a factorization procedure, by which the cross section of these processes is separated into a short-distance quark/gluon subprocess, calculable in perturbative QCD, and the distribution of the partons in the initial state, and thus represent long-distance, low-energy characteristics of the nucleon. As such, they are governed by the same low-energy dynamics which determines other nucleon observables like the vector and axial couplings (to which they are related by the partonic sum rules), form factors, meson-nucleon couplings *etc.* Of particular interest are the charge ($u - \bar{u}, d - \bar{d}$) and flavor

$(u - d, \bar{u} - \bar{d})$ non-singlet quark densities, which exhibit only weak scale dependence and are of non-perturbative origin; they represent quasi-observables which directly probes the QCD quark structure of the nucleon at low resolution scales.

The long-distance behavior of strong interactions at low energies is governed by the spontaneous breaking of chiral symmetry in QCD. The Goldstone boson nature of the pion explains its small mass on the hadronic scale and requires its coupling to other hadrons to vanish in the long-wavelength limit. The resulting “chiral dynamics” gives rise to a number of distinctive phenomena at distance scales $\sim 1/M_\pi$, such as the $\pi\pi, \pi N$ and NN interaction at large distances, the pion pole in the axial current matrix element, *etc.* An important question is how chiral dynamics affects the nucleon’s parton densities, and whether one can see any signs of chiral effects in observables of high-momentum transfer processes.

The prime candidate for an effect of chiral dynamics in parton densities has been the flavor asymmetry of the light antiquark densities in the nucleon. Measurements of the proton-neutron structure function difference in inclusive deep-inelastic scattering [1], semi-inclusive meson production [2], and particularly Drell-Yan pair production [3, 4, 5] have unambiguously shown that $[\bar{d} - \bar{u}](x) > 0$ in the proton for $x < 0.3$, and have partly mapped the x -dependence of the asymmetry; see Refs. [6] for a review of earlier experimental results. The basic picture is that the “bare” proton can make a transition to a virtual state containing a pion, and fluctuations $p \rightarrow n\pi^+$ are more likely than $p \rightarrow \Delta^{++}\pi^-$, resulting in an excess of π^+ over π^- in the “dressed” proton. Following the original prediction of Ref. [7], which included only the nucleon intermediate state, this idea was implemented in a variety of dynamical models, which incorporate finite-size effects through various types of hadronic form factors associated with the πNN and $\pi N\Delta$ vertices; see Refs. [6] for a review of the extensive literature. It was noted long ago [8] that in order to reproduce the fast decrease of the observed asymmetry with x one needs πNN form factors much softer than those commonly used in meson exchange parametrizations of the NN interaction [9]. However, even with such soft form factors the pion transverse momenta in the nucleon generally extend up to values $\gg M_\pi$ [10]. This raises the question to what extent such models actually describe long-distance effects associated with soft pion exchange (momenta $\sim M_\pi$), and what part of their predictions is simply a parametrization of short-distance dynamics which should more naturally be described in terms of non-hadronic degrees of freedom. More generally, one faces the question how to formulate the concept of the “pion cloud” in the nucleon’s partonic structure [11] in a manner consistent with chiral dynamics in QCD.

A framework which allows one to address these questions in a systematic fashion is the transverse coordinate (or impact parameter) representation, in which the distribution of partons is studied as a function of the

longitudinal momentum fraction, x , and the transverse distance, b , of the parton from the transverse center-of-momentum of the nucleon [12, 13]. In this representation, chiral dynamics can be associated with a distinct component of the partonic structure, located at $x \lesssim M_\pi/M_N$ and $b \sim 1/M_\pi$. In a previous work [14] we have shown that in the gluon density this large-distance component is sizable and causes the nucleon’s average gluonic transverse size, $\langle b^2 \rangle_g$ to grow if x drops below M_π/M_N , in agreement with the t -slopes observed in exclusive J/ψ photo- and electroproduction at HERA [15, 16], FNAL [17], and experiments at lower energies. Essential in this is the fact that in the gluon density (more generally, in any isoscalar parton density) the pion cloud contributions from N and Δ intermediate states have the same sign and add constructively. The special role of the Δ compared to other excited baryon states is supported by the fact that in the large- N_c limit of QCD the N and Δ are degenerate and enter on an equal footing.

In this article we perform a comprehensive study of the chiral large-distance component of the nucleon’s partonic structure, considering both its contribution to the total quark/antiquark/gluon densities and to the nucleon’s average partonic transverse size. The method we use to calculate this component is phenomenological pion exchange formulated in the impact parameter representation, restricted to the region of large transverse distances. A physical lower limit in b for πB ($B = N, \Delta$) configurations in the nucleon wave function is set by the transverse “core” radius, estimated from the nucleon’s axial form factor, $R_{\text{core}} = 0.55 \text{ fm}$, and we explicitly demonstrate the universal character of the pionic contributions in the region $b > R_{\text{core}}$. This formulation preserves the basic physical picture of the “pion cloud” model of the nucleon’s sea quark distributions, while restricting its application to the region actually governed by chiral dynamics. In fact, our study serves both a conceptual and a practical purpose. First, we want to establish in which region of transverse distances the results of the traditional pion cloud model are model-independent and can be associated with large-distance chiral dynamics. Second, we want to employ this model to actually calculate the universal large-distance component and study its properties. A preliminary account of our study of the flavor asymmetry $\bar{d} - \bar{u}$ was presented in Ref. [18].

The investigation reported here proceeds in several steps. In Sec. II, we develop the theory of large-distance contributions to the partonic structure from a general, model-independent perspective. We outline the parametric region of πB configurations in the nucleon wave function, the properties of the b -dependent momentum distribution of pions in the nucleon, its large- b asymptotics, and the convolution formulas for the nucleon parton densities. In Sec. III, we investigate the phenomenological pion cloud model in the impact parameter representation, and demonstrate that at large b its predictions become independent of the πNB form factors modeling the short-distance dynamics. We also comment on the

extension of this model to $SU(3)$ flavor. In Sec. IV we then apply this model to calculate the large-distance contributions to the sea quark distributions in the nucleon, including the isovector ($\bar{d} - \bar{u}$) and isoscalar ($\bar{u} + \bar{d}$) light quark sea, the strange sea (s, \bar{s}), and the $SU(3)$ -flavor symmetry breaking asymmetry ($\bar{u} + \bar{d} - 2\bar{s}$). We compare the calculated large-distance contributions to empirical parametrizations of the parton densities and thus indirectly infer the contribution from the short-distance region (“core”), which cannot be calculated in a model-independent way. In the course of this we see how the restriction to large b solves several problems inherent in the traditional pion cloud model which formally allows for pionic configurations also at small impact parameters. In Sec. V we consider the large-distance contributions to the nucleon’s partonic transverse size $\langle b^2 \rangle$, which is accessible experimentally through the t -slope of hard exclusive processes $\gamma^* N \rightarrow M + N$ ($M = \text{meson}, \gamma, \text{etc.}$). Because of the emphasis on large distances this quantity is calculable in a practically model-independent manner and represents a clean probe of chiral dynamics in the partonic structure. Specifically, we show that at $x \sim 10^{-2}$ the large-distance contribution to the nucleon’s singlet quark transverse size, $\langle b^2 \rangle_{q+\bar{q}}$, is larger than that to the gluonic size, $\langle b^2 \rangle_g$, which is consistent with the observation of a larger t -slope in deeply-virtual Compton scattering [19, 20] than in exclusive J/ψ production at HERA [15, 16]. In Sec. VI we discuss the correspondence of the phenomenological pion exchange contribution to the nucleon parton densities with the large- N_c limit of QCD. In particular, we show that the large-distance contributions obtained from pion exchange reproduce the general N_c -scaling of parton densities in QCD, thanks to the degeneracy of N and Δ intermediate states in the large- N_c limit. This re-affirms the need to include intermediate Δ states on the same footing as the nucleon, and shows that the phenomenological large-distance contributions considered here are a legitimate part of the nucleons partonic structure in large- N_c QCD. Finally, in Sec. VII we focus on the physical limitations to the picture of individual πB configurations at small x , arising from the non-chiral growth of the transverse sizes due to diffusion, and from chiral corrections to the structure of the pion. We also comment on the role of chiral dynamics at large longitudinal distances. Our summary and outlook are presented in Sec. VIII. The two appendices present technical material related to the meson-nucleon coupling constants for $SU(3)$ flavor symmetry, and the numerical evaluation of the b -dependent pion momentum distributions in the nucleon.

In the context of our studies of the strange sea quark distributions, $s(x)$ and $\bar{s}(x)$, and the $SU(3)$ flavor symmetry-breaking asymmetry, $[\bar{u} + \bar{d} - 2\bar{s}](x)$, we consider also contributions from configurations containing $SU(3)$ octet mesons ($K\Lambda, K\Sigma, K\Sigma^*, \eta N$) to the nucleon’s partonic structure at large distances. While such high-mass configurations are not governed by chiral dynamics and treated at a purely phenomenological level, it

is interesting to compare their large-distance tails with those of chiral contributions from pions. We note that the issue of the strange sea in the nucleon (s, \bar{s}) and the question of possibly different x -distributions of s and \bar{s} has acquired new urgency following the results of the NuTeV experiment in semi-inclusive charged-current neutrino DIS, which can discriminate between s and \bar{s} via the process $W^+ + s \rightarrow c$ [21, 22].

Chiral contributions to the nucleon’s parton densities have been studied extensively within chiral perturbation theory [23, 24], mostly with the aim of extrapolating lattice QCD results obtained at large pion masses toward lower values [25]. Chiral perturbation theory was also applied to GPDs, including the impact parameter representation [26, 27, 28, 29]. Compared to these calculations, which use methods of effective field theory based on a power-counting scheme, we take here a more pragmatic approach. We study the pion distribution in the nucleon in a phenomenological approach which incorporates the finite bare nucleon size through form factors, and investigate numerically in which region the results become insensitive to the form factors and can be attributed to universal chiral dynamics [62]. In this approach we maintain exact relativistic kinematics (physical pion and nucleon masses) and calculate distributions of finite support, which are then analyzed in the different parametric regions and matched with the asymptotic “chiral” predictions. This also allows us to deal with the strong cancellations between contributions from N and Δ intermediate states in the isovector quark densities, which are difficult to accommodate within a power counting scheme. In fact, the cancellation becomes exact in the large- N_c limit of QCD and ensures the proper $1/N_c$ counting required of the isovector antiquark distribution in QCD [14].

In this study we focus on chiral large-distance contributions to the nucleon’s partonic structure at moderately small momentum fractions, $x \gtrsim 10^{-2}$, which arise from individual πB ($B = N, \Delta$) configurations in the nucleon wave function. When extending the discussion toward smaller x , several effects need to be taken into account which potentially modify this picture. One is diffusion in the partonic wave function, which causes the transverse size of the nucleon’s partonic configurations to grow at small x (however, this effect is suppressed at large Q^2). Another effect are possible chiral corrections to the structure of the pion itself, which were recently studied in an approach based on resummation of chiral perturbation theory in the leading logarithmic approximation [31]. We discuss the limitations to the applicability of the picture of individual πB configurations in Secs. VII A and VII B. We also comment on the role of πB configurations at large longitudinal separations and arbitrary transverse distances, and point out that there may be a window for a chiral regime at $x \gtrsim 10^{-2}$; at smaller x coherence effects become dominant; see Sec. VII C. A detailed investigation of this new regime will be the subject of a separate study.

II. CHIRAL DYNAMICS AND PARTONIC STRUCTURE

A. Parametric region of chiral component

As the first step of our study we want to delineate the parametric region where parton densities are governed by chiral dynamics and establish its numerical limits, as imposed by other, non-chiral physical scales. The primary object of our discussion is the pion longitudinal momentum and transverse coordinate distribution in a fast-moving nucleon, $f_\pi(y, b)$, where y is the pion momentum fraction. Here we introduce this concept heuristically, appealing to its obvious physical meaning; its precise definition in terms of GPDs and its region of applicability will be elaborated in the following.

Chiral dynamics generally governs contributions to nucleon observables from large distances, of the order $1/M_\pi$, which is assumed here to be much larger than all other hadronic length scales in question. These contributions result from exchange of “soft” pions in the nucleon rest frame; in the time-ordered formulation of relativistic dynamics these are pions with energies $E_\pi \sim M_\pi$ and momenta $|\mathbf{k}_\pi| \sim M_\pi$. Chiral symmetry provides that such pions couple weakly to the nucleon and to each other, so that their effects can be computed perturbatively. Boosting these weakly interacting pion-nucleon configurations to a frame in which the nucleon is moving with large velocity, we find that they correspond to longitudinal pion momentum fractions of the order [63]

$$y \sim M_\pi/M_N. \quad (1)$$

At the same time, the soft pions’ transverse momenta, which are not affected by the boost, correspond to transverse distances of the order

$$b \sim 1/M_\pi. \quad (2)$$

Together, Eqs. (1) and (2) determine the parametric region where the pion distribution in the fast-moving nucleon is governed by chiral dynamics, and the soft pion can be regarded as a “parton” in the nucleon’s wave function in the usual sense (see Fig. 1).

The condition Eq. (1) implies that the pion momentum fraction in the nucleon is parametrically small, $y \ll 1$, *i.e.*, the soft pion is a “slow” parton. As a consequence, one can generally neglect the recoil of the spectator system and identify the distance b with the separation of the pion from the transverse center-of-momentum of the spectator system, $r = b/(1 - y)$ [64] [12]. This circumstance greatly simplifies the spatial interpretation of chiral contributions to the parton densities.

Pionic configurations in the nucleon wave function are physically meaningful only if the transverse separation of the pion and the spectator system is larger than the sum of the intrinsic “non-chiral” sizes of these objects. This basic fact imposes a limit on the applicability of chiral dynamics, even though the dynamics itself may not

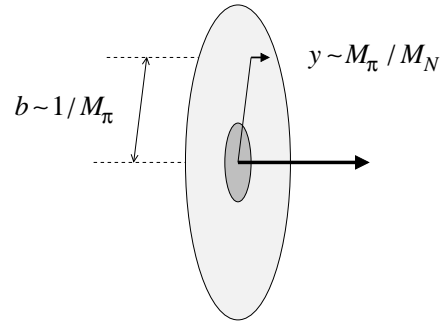


FIG. 1: Parametric region where the pion distribution in the nucleon is governed by chiral dynamics. The variables are the pion longitudinal momentum fraction, y , and transverse position, b .

change dramatically at the limiting distance. In order to make the picture of Fig. 1 quantitative, we have to estimate down to which values of b the concept of pionic configurations is applicable.

The transverse size of the “core” in the nucleon’s partonic wave function in the valence region ($x \gtrsim 10^{-1}$) can be estimated from the transverse axial charge radius of the nucleon, which does not receive contributions from the pion cloud [14, 32]:

$$\langle b^2 \rangle_{\text{axial}} = \frac{2}{3} \langle r^2 \rangle_{\text{axial}} \approx 0.3 \text{ fm}^2, \quad (3)$$

where the factor $2/3$ results from converting the 3-dimensional charge radius in the rest frame into the 2-dimensional transverse charge radius in the frame where the nucleon is moving fast. Identifying the core radius with the transverse RMS radius, we obtain

$$R_{\text{core}} = [\langle b^2 \rangle_{\text{axial}}]^{1/2} \approx 0.55 \text{ fm}. \quad (4)$$

Equation (4) imposes a numerical lower limit for the pion impact parameter, b , in pionic configurations. Note that this number represents a rough estimate, as the interpretation of RMS radius in terms of a “size” depends on the shape of the transverse distribution of partons in the core. A more refined estimate, which takes into account the intrinsic transverse size of the pion as well as the effect of the recoil of the spectator system, is obtained by requiring that $b/(1 - y) > (R_{\text{core}}^2 + R_\pi^2)^{1/2}$. Assuming that R_π^2 ranges between zero and R_{core}^2 , and anticipating that the typical y -values in the pion distribution at $b \sim R_{\text{core}}$ are $y = (1 - 2) \times M_\pi/M_N \sim 0.2$, we obtain $b > 0.44 - 0.62 \text{ fm}$, in good agreement with the estimate of Eq. (4). When considering the nucleon’s partonic structure at small x ($< 10^{-2}$) the above estimate of the nucleon core size needs to be modified to account for the non-chiral growth due to diffusion in the partonic wave function. Also, in this region the transverse size of the pion itself can grow due to chiral corrections. These effects will be discussed separately in Secs. VII A and VII B.

Chiral dynamics produces also configurations in the fast-moving nucleon characterized by large longitudinal separations of the pion and the spectator system,

$$l \sim 1/M_\pi, \quad (5)$$

with no restriction on b . The relevance of these configurations for the nucleon's partonic structure cannot be ascertained without detailed consideration of the effective longitudinal sizes of the subsystems and possible coherence effects, and will be discussed in Sec. VII C. In the following we limit ourselves to chiral contributions at large transverse distances.

B. Pion distribution in the nucleon

In its region of applicability defined by Eqs. (1) and (2), the b -dependent pion “parton” distribution can be calculated as the transverse Fourier transform of the “pion GPD” in the nucleon. The latter is defined as the transition matrix element of the operator measuring the number density of pions with longitudinal momentum fraction y in the fast-moving nucleon, integrated over the pion transverse momenta, and with a transverse momentum transfer Δ_\perp to the nucleon (see Fig. 2a):

$$\begin{aligned} & \int \frac{d^3 k}{(2\pi)^3} \delta(y - k_\parallel/P) \\ & \times \langle \mathbf{p}_2 | a_{\pi,a}^\dagger(\mathbf{k} + \Delta/2) a_{\pi,a}(\mathbf{k} - \Delta/2) | \mathbf{p}_1 \rangle_{P \rightarrow \infty} \\ & = (2\pi)^3 (2P) \delta^{(3)}(\mathbf{p}_2 - \mathbf{p}_1 + \Delta) H_\pi(y, t), \end{aligned} \quad (6)$$

where $p_{1\parallel} = P \rightarrow \infty$, $\Delta_\parallel = 0$, and

$$t \equiv -\Delta_\perp^2. \quad (7)$$

Here $a_{\pi,a}^\dagger$ and $a_{\pi,a}$ denote the pion creation and annihilation operators, and the sum over isospin projections (subscript a) is implied. Eq. (6) refers to the helicity-conserving component of the nucleon transition matrix element ($\lambda_2 = \lambda_1$), and $H_\pi(y, t)$ is the corresponding GPD; the helicity-flip GPD is defined in analogously but will not be needed in the present investigation. In terms of the pion GPD the transverse coordinate distribution is then obtained as ($b \equiv |\mathbf{b}|$)

$$f_\pi(y, b) = \int \frac{d^2 \Delta_\perp}{(2\pi)^2} e^{-i(\Delta_\perp \cdot \mathbf{b})} H_\pi(y, t). \quad (8)$$

We note that a manifestly covariant definition of the pion GPD, as the matrix element of a pionic light-ray operator between nucleon states, was given in Ref. [14]; the equivalence of that definition to Eq. (6) is shown by going to the frame where the nucleon is moving fast and expanding the pion fields in creation and annihilation operators.

The pion GPD in the nucleon implies summation over all relevant baryonic intermediate states. Because the

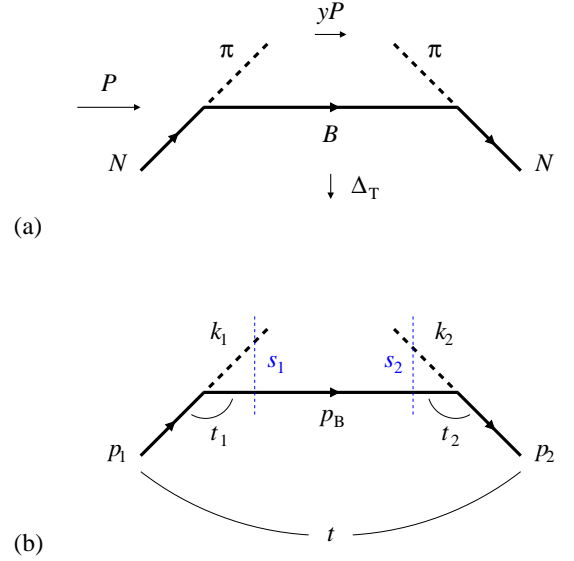


FIG. 2: The pion GPD in the nucleon. (a) Transition matrix element of the density of pions with longitudinal momentum fraction $y \sim M_\pi/M_N$ and transverse momentum transfer $|\Delta_\perp| \sim M_\pi$, Eq. (6). (b) Invariants used in modeling finite-size effects with form factors. $t_{1,2}$ are the pion virtualities in the invariant formulation, Eq. (11); $s_{1,2}$ the invariant masses of the πB systems in the time-ordered formulation, Eq. (20).

pion wavelength is assumed to be large compared to the typical nucleon/baryon radius, only the lowest-mass excitations can effectively contribute to the GPD in the region of Eqs. (1) and (2). We therefore retain only the N and Δ intermediate states in the sum:

$$H_\pi = H_{\pi N} + H_{\pi \Delta}, \quad (9)$$

$$f_\pi = f_{\pi N} + f_{\pi \Delta}. \quad (10)$$

The inclusion of the Δ , whose mass splitting with the nucleon introduces a non-chiral scale which is numerically comparable to the pion mass, represents a slight departure from strict chiral dynamics but is justified by the numerical importance of this contribution; *cf.* the discussion of the $N_c \rightarrow \infty$ limit in QCD in Sec. VI.

To study the properties of the b -dependent pion distribution at large distances we need a dynamical model which allows us to calculate the pion GPD in the relevant region of momenta. Here we follow a heuristic approach and start from the simplest possible system of pointlike pions and nucleons interacting according to a phenomenological Lagrangian. We shall see later how this definition can be amended to incorporate finite-size effects. In which region the results should be regarded as physical in the light of the discussion in Sec. II A will be the matter of the following investigations.

The pion GPD in the nucleon can be calculated using invariant perturbation theory, by evaluating the matrix element in Eq. (6), or, equivalently, the matrix element of the pionic light-ray operator of Ref. [14], using the Feynman rules for pointlike πN interactions; see Ref. [14] for

details. The resulting Feynman integral is computed by introducing light-cone coordinates and performing the integral over the “minus” (energy) component of the loop momentum using Cauchy’s theorem. Closing the contour around the pole of the propagator of the spectator baryon, one arrives at a representation in which the spectator is on mass-shell, and the emitted and absorbed pion are off mass-shell, with virtualities [65]

$$t_{1,2} \equiv k_{1,2}^2 = -(\mathbf{k}_\perp \mp \bar{y} \Delta_\perp / 2)^2 / \bar{y} + t_{\min} \quad (11)$$

(see Fig. 2b). Here \mathbf{k}_\perp is the transverse momentum of the spectator baryon,

$$\bar{y} \equiv 1 - y, \quad (12)$$

and

$$t_{\min} \equiv -[y^2 M_N^2 + y(M_B^2 - M_N^2)] / \bar{y} \quad (13)$$

is the minimum virtuality required by kinematics for a given pion momentum fraction, y . The πN and $\pi \Delta$ GPDs are then obtained as

$$H_{\pi N}(y, t) = 3g_{\pi NN}^2 I_8(y, t; M_\pi, M_N), \quad (14)$$

$$H_{\pi \Delta}(y, t) = 2g_{\pi N\Delta}^2 I_{10}(y, t; M_\pi, M_\Delta). \quad (15)$$

Here $g_{\pi NN}$ and $g_{\pi N\Delta}$ are the coupling constants in the conventions of Ref. [14] and Appendix A, and the distributions are the isoscalar pion GPDs, corresponding to the sum of π^+ , π^- and π^0 distributions in the proton; *cf.* Eq. (6). The functions I_8 and I_{10} denote the basic transverse momentum integrals arising in the calculation of the meson distribution with intermediate octet and decuplet baryons,

$$I_{8,10}(y, t; M_\pi, M_B) \equiv \frac{y}{4\pi\bar{y}} \int \frac{d^2 k_\perp}{(2\pi)^2} \frac{\phi_{8,10}}{(t_1 - M_\pi^2)(t_2 - M_\pi^2)}, \quad (16)$$

where

$$\phi_8 \equiv \frac{1}{2} [-t_1 - t_2 + \bar{y}t + 2(M_B - M_N)^2], \quad (17)$$

$$\begin{aligned} \phi_{10} \equiv & \frac{1}{24 M_N^2 M_\Delta^2} [2M_\Delta^2(-t_1 - t_2 + t) \\ & + (M_N^2 - M_\Delta^2 - t_1)(M_N^2 - M_\Delta^2 - t_2)] \\ & \times [2(M_\Delta + M_N)^2 - t_1 - t_2 + \bar{y}t]. \end{aligned} \quad (18)$$

Note that while the $t_{1,2}$ of Eq. (11) depend on the vector Δ_\perp , the integral Eq. (16) depends only on $t \equiv -\Delta_\perp^2$ because of rotational invariance in transverse space.

As it stands, the transverse momentum integral in Eqs. (16)–(18) is divergent. This divergence is related to short-distance contributions in the pointlike particle approximation and does not affect the chiral long-distance behavior of the b -dependent distribution. Several ways of regularizing this divergence and extracting the chiral contribution will be discussed in the following.

The pion GPD can equivalently be evaluated in time-ordered perturbation theory, where Fig. 2a is interpreted as a process where the fast-moving nucleon (momentum $P \gg M_N$) makes a transition to a πB intermediate state, in which we evaluate the operator measuring the density of pions with longitudinal momentum yP , and then back to a nucleon state whose transverse momentum differs from the original one by Δ_\perp . In this formulation the intermediate particles are on mass-shell, but the energies of the πB states before and after the operator are different from that of the initial/final nucleon state. The invariant masses of the intermediate states, which are directly proportional to the energies, are given by

$$s_{1,2} = (k_{1,2} + p_B)^2 \quad (19)$$

$$= \frac{(\mathbf{k}_\perp \mp \Delta_\perp / 2)^2 + M_\pi^2}{y} + \frac{\mathbf{k}_\perp^2 + M_B^2}{\bar{y}} - \frac{\Delta_\perp^2}{4} \quad (20)$$

(see Fig. 2b). The connection to the invariant formulation is established by noting that, for given y and \mathbf{k}_\perp ,

$$\Delta s_{1,2} \equiv s_{1,2} - M_N^2 = \frac{M_\pi^2 - t_{1,2}}{y}, \quad (21)$$

whence the denominators in Eq. (16) can also be interpreted as “energy denominators.” The minimum value of the invariant mass difference, Δs_{\min} , for given momentum fraction y can be obtained by substituting $t_{1,2}$ by t_{\min} , Eq. (13). Both the invariant and the time-ordered formulation will be useful for discussing the properties of the chiral long-distance contribution following from Eqs. (16)–(18).

C. Large- b asymptotics

It is instructive to consider the asymptotic behavior of the distribution of pions for $b \rightarrow \infty$ and fixed y . It is determined by the leading branch cut singularity of the GPD in the t -channel and can be calculated by applying the Cutkosky rules to the Feynman graphs of Fig. 2 with pointlike vertices [14]. The asymptotic behavior is of the form

$$f_{\pi B}(y, b) \propto \frac{e^{-\kappa_B b}}{\kappa_B b}, \quad (22)$$

where $B = N, \Delta, \dots$ denotes the intermediate baryon; the expression applies in principle also to higher-mass states, *cf.* the discussion below. The decay constant, κ_B , depends on the pion momentum fraction, y , and is directly related to the minimum pion virtuality, Eq. (13), in the invariant formulation, or the minimum invariant mass difference in the time-ordered formulation, *cf.* Eq. (21):

$$\kappa_B = 2 \left(\frac{M_\pi^2 - t_{\min}}{\bar{y}} \right)^{1/2}. \quad (23)$$

To exhibit the y -dependence of the decay constant in the parametric region of chiral dynamics, $y \sim M_\pi/M_N$,

Eq. (1), we set

$$y = \eta M_\pi/M_N, \quad (24)$$

where the scaling variable, η , is generally of order unity. Substituting Eq. (13) into Eq. (23) and dropping terms suppressed by powers of M_π/M_N , we obtain

$$\kappa_B = 2 \left[(1 + \eta^2) M_\pi^2 + \eta \frac{(M_B^2 - M_N^2) M_\pi}{M_N} \right]^{1/2}. \quad (25)$$

This result has several interesting implications:

- (a) For the nucleon intermediate state ($B = N$) the second term is zero, and one has $\kappa_N \propto M_\pi$ with a coefficient of order unity and depending on η . In this case the b -distribution exhibits a “Yukawa tail” with a y -dependent range of the order $1/M_\pi$, as expected.
- (b) For a higher-mass intermediate state ($B \neq N$) the decay constant is determined by competition of the chiral scale, M_π^2 , and the non-chiral scale, $(M_B^2 - M_N^2) M_\pi/M_N$. The larger the N - B mass splitting, the smaller η has to be for the chiral scale to dominate. This effect suppresses the contribution of higher-mass baryons to $f_\pi(y, b)$ at large b and finite η . Note also that the pre-exponential factor, which is not shown in Eq. (22) for brevity, vanishes $\propto y$ for $y \rightarrow 0$ [14].
- (c) For $\eta \rightarrow 0$ one finds $\kappa_B \rightarrow 2M_\pi$ irrespective of the N - B mass splitting. In this limit the transverse “Yukawa tail” has the range one would naively expect from the analogy with the 3-dimensional situation. However, this limit is purely formal, as this region makes a vanishing contribution to the nucleon’s partonic structure at moderate x ; cf. the discussion in Secs. II D and VII below.

For pion momentum fractions parametrically of order unity, $y \sim 1$, Eq. (23) gives a decay constant of the order $\kappa_B \sim M_N$. An exponential decay with range $\sim 1/M_N$ is not a chiral contribution to the pion distribution, as is expected, because the values of y lie outside the parametric region of Eq. (1). In sum, the large- b asymptotic behavior obtained from the naive pion distribution with pointlike πN couplings fully supports the general arguments of Sec. II A concerning the parametric region of the chiral component.

One notes that the characteristic transverse range of the chiral contribution of the pion distribution, $1/(2M_\pi) = 0.71 \text{ fm}$, is numerically not substantially larger than our estimate of the non-chiral “core” size, Eq. (4). This shows that an effective field theory approach to chiral dynamics, which implicitly assumes that the core has zero size and builds up its structure by counter terms, is not practical here, and underscores the rationale for our phenomenological approach, where finite-size effects are included explicitly.

D. Contribution to nucleon parton densities

The chiral contribution to the nucleon’s parton densities is obtained as the convolution of the pion momentum distribution in the nucleon with the relevant parton distribution in the pion. For the gluon, the isoscalar quark/antiquark, and the isovector quark/antiquark densities it takes the form [66]

$$g(x, b)_{\text{chiral}} = \int_x^1 \frac{dy}{y} [f_{\pi N} + f_{\pi \Delta}] (y, b) g_\pi(z), \quad (26)$$

$$\begin{aligned} [u + d] (x, b)_{\text{chiral}} &= [\bar{u} + \bar{d}] (x, b)_{\text{chiral}} \\ &= \int_x^1 \frac{dy}{y} [f_{\pi N} + f_{\pi \Delta}] (y, b) q_\pi^{\text{tot}}(z), \end{aligned} \quad (27)$$

$$\begin{aligned} [u - d] (x, b)_{\text{chiral}} &= [\bar{d} - \bar{u}] (x, b)_{\text{chiral}} \\ &= \int_x^1 \frac{dy}{y} \left[\frac{2}{3} f_{\pi N} - \frac{1}{3} f_{\pi \Delta} \right] (y, b) q_\pi^{\text{val}}(z), \end{aligned} \quad (28)$$

where

$$z \equiv x/y \quad (29)$$

is the parton momentum fraction in the pion. Here $f_{\pi N}$ and $f_{\pi \Delta}$ are the isoscalar pion distributions (sum of π^+ , π^- and π^0) with N and Δ intermediate states in the conventions of Refs. [10, 14] and Appendix A; the isovector nature of the asymmetry, Eq. (28), is encoded in the numerical prefactors. The functions g_π , q_π^{tot} , and q_π^{val} are the gluon, isoscalar (total), and isovector (valence) quark/antiquark densities in the pion,

$$\begin{aligned} q_\pi^{\text{tot}}(z) &= [\bar{u} + \bar{d}]_{\pi^\pm, \pi^0}(z) = [u + d]_{\pi^\pm, \pi^0}(z) \\ &= \frac{1}{2} [u + \bar{u} + d + \bar{d}]_{\pi^\pm, \pi^0}(z), \end{aligned} \quad (30)$$

$$\begin{aligned} q_\pi^{\text{val}}(z) &= \pm [\bar{d} - \bar{u}]_{\pi^\pm}(z) = \pm [u - d]_{\pi^\pm}(z) \\ &= \pm \frac{1}{2} [u - \bar{u} - d + \bar{d}]_{\pi^\pm}(z); \end{aligned} \quad (31)$$

the latter is normalized as

$$\int_0^1 dz q_\pi^{\text{val}}(z) = 1. \quad (32)$$

The π^0 does not have a valence distribution because of charge conjugation invariance, and we assume isospin symmetry. Note that the parton densities in the pion, as well as the result of the convolution integrals in Eqs. (26)–(28), depend on the resolution scale; we have suppressed this dependence for brevity. The convolution formulas for the strange antiquark density and the $SU(3)$ -flavor symmetry breaking asymmetry will be given in Sec. IV.

The expressions in Eqs. (26)–(28) apply to parton momentum fractions of the order $x \sim M_\pi/M_N$ but otherwise not exceptionally small, and transverse distances

$b \sim 1/M_\pi$. In deriving them we have assumed that the “decay” of the pion into partons happens locally on the transverse distance scale of the chiral b -distribution, $b \sim 1/M_\pi$ (see Fig. 1). This is justified parametrically, as for the values of x under consideration the parton momentum fraction in the pion does not reach small values ($x < z < 1$ in the convolution integral) and one can neglect chiral effects which cause the size of the pion itself to grow at small z .

To see in which region of x the chiral contribution to the isovector antiquark density is localized, it is convenient to write the convolution formula Eq. (28) in the form

$$x [\bar{d} - \bar{u}] (x, b)_{\text{chiral}} = \int_x^1 dy \left[\frac{2}{3} f_{\pi N} - \frac{1}{3} f_{\pi \Delta} \right] (y, b) \times z q_\pi^{\text{val}}(z), \quad (33)$$

where we have multiplied both sides of Eq. (28) by x and used Eq. (29) on the right-hand side. Now both functions in the integrand vanish for small arguments: $f_{\pi B}(y) \rightarrow 0$ for $y \rightarrow 0$, and $z q_\pi^{\text{val}}(z) \rightarrow 0$ for $z \rightarrow 0$. Noting that the valence distribution $z q_\pi^{\text{val}}(z)$ is localized around $z \sim 1/2$ at low scales, and that the pion momentum distribution is centered around $y \sim M_\pi/M_N$, we conclude that the convolution produces a sea quark distribution in the nucleon centered around values $x = yz \sim (1/2) \times M_\pi/M_N$, in agreement with the general expectation. The same argument applies to the bulk of the chiral isoscalar density, Eq. (27), which arises mainly from the valence quark content of the pion; only at very small x the non-valence quarks in the pion produce a distinct contribution. Note also that the valence quark density in the pion at $z \sim 1/2$ is generated mostly by relatively small-size configurations in the pion, justifying our approximation of neglecting the intrinsic transverse size of the pion in the convolution integrals.

One immediately sees from Eqs. (27) and (28) that the chiral large-distance component is larger in the isoscalar than in the isovector quark distributions, because the N and Δ contributions add in the isoscalar sector, Eq. (27), while they partly cancel in the isovector sector, Eq. (28) [10]. This is contrary to the general expectation that chiral effects manifest themselves mostly in the sea quark flavor asymmetry $\bar{d} - \bar{u}$. The cancellation between N and Δ contributions in the isovector case becomes perfect in the large- N_c limit of QCD and restores the proper N_c scaling of the isovector distributions; see Sec. VI.

In principle one can use the asymptotic expressions for the pion distribution in the nucleon, Eqs. (22) and (23), to do a numerical estimate of the large-distance contribution to the nucleon parton densities based on Eqs. (26)–(28). This approach was taken in Ref. [14] to estimate the chiral contribution to the nucleon’s gluonic transverse size, $\langle b^2 \rangle_g$, proportional to the b^2 -weighted integral of the impact-parameter dependent gluon density. Because of the weighting with b^2 this quantity emphasizes large transverse distances, and the estimates of the

b -integrated chiral contribution are relatively insensitive to the lower limit in b imposed in the integral (see also Sec. V). In the present investigation we are interested in the antiquark densities *per se* (not weighted with b^2), where there is no such enhancement of large distances, and estimates of the chiral contribution are more sensitive to the lower limit in b . We therefore approach this problem differently, by analyzing the phenomenological pion cloud model (which incorporates finite-size effects) and establishing down to which b the numerical predictions are insensitive to the short-distance cutoff (Sec. III). The numerical evaluation of the long-distance contribution based on Eqs. (26)–(28) will then be done based on the results of this investigation (Secs. IV and V).

III. PION CLOUD MODEL IN IMPACT PARAMETER REPRESENTATION

A. Modeling finite-size effects

For a quantitative study of the chiral large-distance component in the nucleon’s partonic structure we need a dynamical model which allows us to compute the distribution of pions beyond its leading asymptotic behavior. In addition, we must address the question down to which values of b numerical study of this component is meaningful, in the sense that it is not overwhelmed by short-distance contributions unrelated to chiral dynamics. Ultimately, this question can only be answered in a dynamical model which smoothly “interpolates” between the chiral long-distance regime and the effective short-distance dynamics. Here we study this question in the framework of the phenomenological pion cloud model, where the short-distance dynamics is not treated explicitly, but modeled by form factors implementing a finite hadronic size unrelated to chiral dynamics. This study serves two purposes — it establishes what part of the predictions of the traditional pion cloud model actually arises from the long-distance region governed by chiral dynamics, and it offers a practical way of computing this universal long-distance contribution.

In the phenomenological pion cloud model, the pion GPD in the nucleon is defined by the graph of Fig. 2, *cf.* Eqs. (16)–(18), in which now form factors are associated with the πNB vertices, rendering the transverse momentum integral explicitly finite. Two different schemes to implement these form factors are commonly used and have extensively been discussed in the literature. One, based on the invariant formulation in which the spectator baryon is on mass-shell, restricts the virtualities of the exchanged pions by inserting in Eq. (16) a form factor

$$\mathcal{F} \left(\frac{M_\pi^2 - t_{1,2}}{\Lambda_{\text{virt}}^2} \right) \quad (34)$$

for each πNB vertex (see Fig. 2b). Here $\mathcal{F}(a)$ denotes a function of finite range which vanishes for $a \rightarrow \infty$;

for example, an exponential, $\exp(-a)$, or the dipole form factor, $(1+a)^{-2}$. These form factors can be compared to those in the well-known meson exchange parametrizations of the NN interaction, where the exchanged pion is regarded as a virtual particle [9]. The other scheme, based on the time-ordered formulation, restricts the invariant mass of the πB systems in the intermediate states by form factors of the type [33]

$$\mathcal{F}\left(\frac{s_{1,2} - M_N^2}{\Lambda_{\text{inv. mass}}^2}\right) \quad (35)$$

(see Fig. 2b). An advantage of this scheme is that it preserves the momentum sum rule in the transition $N \rightarrow \pi B$, *i.e.*, the longitudinal momentum distribution of the baryon B in the nucleon is given by $f_{\pi B}(1-y)$ for $B = N, \Delta$ [33, 34]. The relation between the two different cutoff schemes can easily be derived from Eq. (21). Effectively,

$$\Lambda_{\text{virt}}^2 = y \Lambda_{\text{inv. mass}}^2, \quad (36)$$

i.e., a constant invariant mass cutoff amounts to a y -dependent virtuality cutoff which tends to zero as $y \rightarrow 0$. In the traditional formulation of the pion cloud model, without restriction to the large- b region, the two schemes lead to rather different pion momentum distributions. The distributions at large b and $y \sim M_\pi/M_N$, however, are dominated by vanishing pion virtualities *viz.* invariant mass differences, so that the results in the two schemes become effectively equivalent, up to small finite renormalization effects. In the following numerical studies we shall employ the virtuality cutoff as used in Ref. [10]; the equivalence of the two schemes for our purposes will be demonstrated explicitly in Sec. III C.

We emphasize that we are interested in the pion cloud model with form factors only as a means to identify the chiral large-distance contribution and delineate the region where it is universal and independent of the form factors. We do not consider those aspects of the model related to the fitting of data without restriction to large distances (tuning of cutoff parameters, πNB couplings, *etc.*); those have been discussed extensively in the literature reviewed in Refs. [6].

B. Universality at large b

We first consider the dependence of the pion distribution in the nucleon on the impact parameter, b . Specifically, we want to demonstrate that it reproduces the “universal” chiral behavior Eq. (22) at large b , and investigate for which values of b the distribution is substantially modified by the form factors. To this end we calculate the pion GPD by numerical evaluation of the loop integral, Eq. (16), with a virtuality cutoff of the type of Eq. (34), and perform the transformation to the impact parameter representation according to Eq. (8); useful formulas for the numerical calculation are collected in

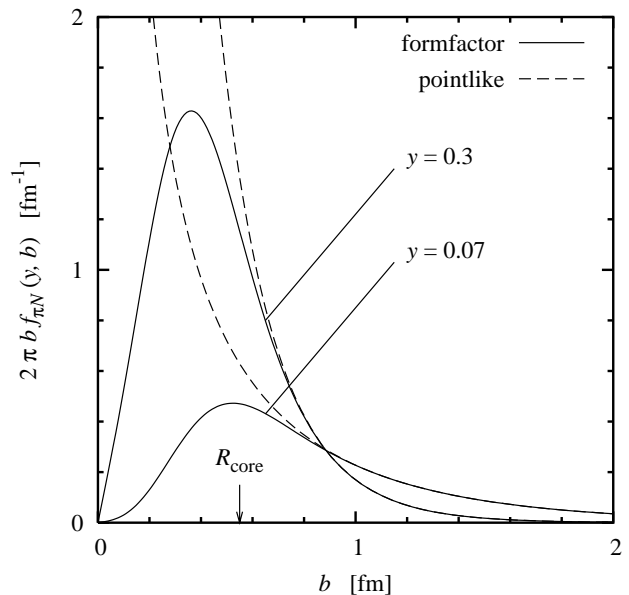


FIG. 3: The transverse spatial distribution of pions in the nucleon, $f_{\pi N}(y, b)$, as a function of b , for values $y = 0.07$ and 0.3 . Shown is the radial distribution $2\pi b f_{\pi N}(y, b)$, whose integral over b (area under the curve) gives the pion momentum distribution. *Solid lines*: Pion cloud model with virtuality cutoff (exponential form factor, $\Lambda_{\pi N} = 1.0$ GeV) [10]. *Dashed line*: Distribution for pointlike particles, regulated by subtraction at $\Delta_\perp^2 = 0$; the integral over b does not exist in this case. The estimated “core” radius, Eq. (4), is marked by an arrow.

Appendix B. Figure 3 shows $f_{\pi N}(y, b)$ obtained with an exponential form factor ($\Lambda_{\text{virt}} = 1.0$ GeV, a typical value in traditional applications of the pion cloud model), as a function of b for $y = 0.07$ and 0.3 , which is $1/2$ and 2 times M_π/M_N , respectively. Also shown are the distributions obtained with pointlike particles (no form factors), in which the loop integral was regularized by subtraction at $\Delta_\perp^2 = 0$; this subtraction of a Δ_\perp^2 -independent term in the GPD corresponds to a modification of the impact parameter distribution by a delta function term $\propto \delta^{(2)}(\mathbf{b})$, which is “invisible” at finite b [14]. One sees that for $b \gtrsim 0.5$ fm the results of the two calculations coincide, showing that in this region the pion distribution is not sensitive to the form factors. Comparison of different functional forms of the form factor (exponential, dipole) also supports this conclusion. Furthermore, we note that for large b both distributions in Fig. 3 exhibit the universal asymptotic behavior derived earlier [14].

It is interesting that the b -value where in Fig. 3 the “universal” behavior of $f_{\pi N}(y, b)$ sets in is numerically close to the transverse radius of the nucleon’s “core,” inferred earlier from independent considerations, $R_{\text{core}} \approx 0.55$ fm, *cf.* Eq. (4). This shows that the pion cloud model can safely be used to compute the large- b parton densities over the entire region defined by Eq. (4).

Figure 4 illustrates the connection between the transverse distance and the pion virtualities in Eq. (16) from

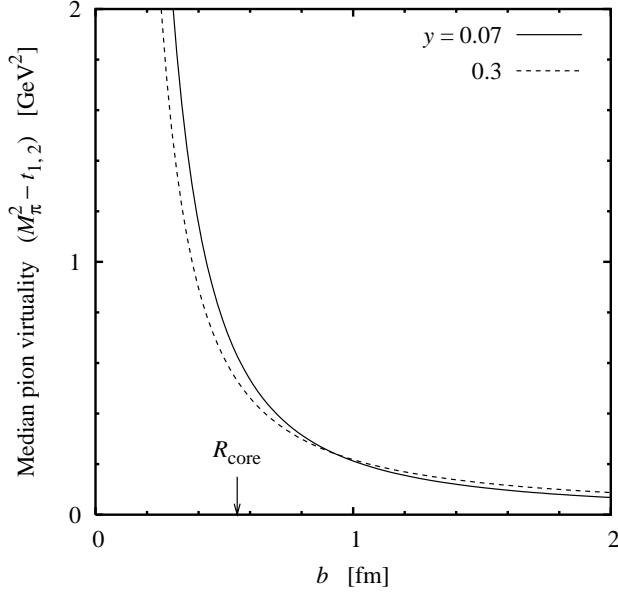


FIG. 4: The median pion virtuality in the unregularized integral, Eqs. (16)–(18), as a function of b , for $y = 0.07$ (solid line) and 0.3 (dotted line). It is defined as the value of the virtuality cutoff, Λ_{virt}^2 , for which $f_{\pi N}(y, b)$ reaches half of its value for $\Lambda_{\text{virt}}^2 \rightarrow \infty$, corresponding to the unregularized integral.

a different perspective. Shown there is the median pion virtuality in the unregularized loop integral, defined as the value of the virtuality cutoff, Λ_{virt}^2 , for which the regularized $f_{\pi N}(y, b)$ reaches half of its value for $\Lambda_{\text{virt}}^2 \rightarrow \infty$; the latter coincides with the value obtained by regularization through subtraction. The function $f_{\pi N}(y, b)$ is always positive when evaluated with an exponential virtuality cutoff, and monotonously decreasing as a function of Λ_{virt}^2 , so that the median value of Λ_{virt}^2 provides a sensible measure of the average virtualities in the integral Eq. (16) for given y and b . One sees that the average pion virtualities in the loop strongly decrease with increasing b , indicating the approach to the universal chiral region. We recall that the leading asymptotic behavior at $b \rightarrow \infty$ is determined by quasi-on-shell pions, *cf.* the derivation in Sec. II C.

C. Effective pion momentum distribution

We now want to investigate the distribution of pions at large transverse distances as a function of the momentum fraction, y . In keeping with our general line of approach, we do this by studying how the momentum distribution of the pion cloud model with form factors is modified when a restriction on the minimum b is imposed. We define the effective momentum distribution of pions with

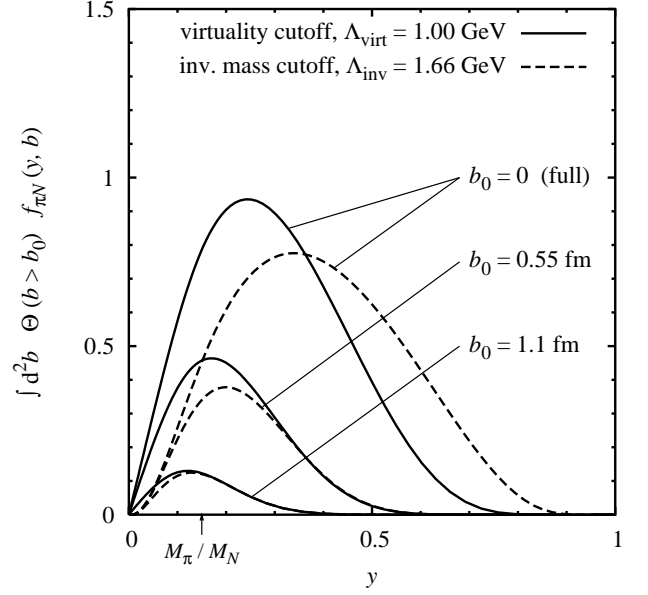


FIG. 5: Effective momentum distribution of pions in πN configurations with impact parameters $b > b_0$, Eq. (37), in the pion cloud model. *Solid lines*: Distributions obtained with a virtuality cutoff, Eq. (34) (exponential form factor, $\Lambda_{\text{virt}} = 1.0$ GeV), for $b_0 = 0$ (full integral), $b_0 = 0.55$ fm and $b_0 = 1.1$ fm. *Dashed lines*: Same for distributions obtained with an invariant mass cutoff, Eq. (34) (exponential form factor, $\Lambda_{\text{virt}} = 1.66$ GeV). The value of Λ_{virt} was chosen such that it produces the same total number of pions (y -integral) for the full distribution as the given virtuality cutoff. The value $y = M_\pi/M_N$ is indicated by an arrow.

$b > b_0$ as the integral

$$\int d^2b \Theta(b > b_0) f_{\pi B}(y, b) \quad (B = N, \Delta); \quad (37)$$

for $b_0 = 0$ we recover the momentum distribution of pions in the traditional usage of the pion cloud model. Figure 5 (solid lines) shows the b -integrated distribution Eq. (37), obtained with an exponential virtuality cutoff ($\Lambda_{\text{virt}} = 1.0$ GeV), for $b_0 = 0$ (full integral) as well as $b_0 = 0.55$ fm and 1.1 fm, corresponding to 1 and 2 times the phenomenological core radius, R_{core} . One sees that the restriction to large b -values strongly suppresses large pion momentum fractions and shifts the strength of the distribution toward values of the order $y \sim M_\pi/M_N$, in agreement with the general expectations formulated in Sec. II. From the perspective of the traditional pion cloud model, the results of Fig. 5 show that less than half of the pions in that model arise from the region $b > R_{\text{core}}$, where the pion cloud can be regarded as a distinct component of the nucleon wave function

Also shown in Figure 5 (dashed lines) are the corresponding distributions obtained with an invariant mass cutoff, Eq. (35). For the sake of comparison the cutoff parameter Λ_{inv}^2 was chosen here such that it gives the same total number of pions (y -integral) for the “full” distri-

butions in which no restriction on b is imposed ($b_0 = 0$); the value of $\Lambda_{\text{inv}} = 1.66 \text{ GeV}$ thus obtained is within the range considered in phenomenological applications of the pion cloud model [35]. One sees that the full distributions are quite different for the virtuality and the invariant mass cutoff, as dictated by the relation (21). However, when restricted to large b the y -distributions in the two regularization schemes become more and more alike, as their strength shifts toward values of the order $y \sim M_\pi/M_N$. This explicitly demonstrates the equivalence of the virtuality and the invariant mass regularization in the context of our approach, as announced above.

D. Extension to $SU(3)$ flavor

In our studies of the strange sea and the $SU(3)$ -breaking flavor asymmetry below we shall consider also the contributions from K and η mesons to the sea quark distributions at large distances. Because the masses of these mesons are numerically comparable to the typical hadronic mass scale (as given, say, by the vector meson mass), their contributions to the partonic structure of the nucleon cannot be associated with chiral dynamics, even at large transverse distances. Still, in the context of the present discussion of the pion cloud model, it is instructive to study the distribution of K and η in the impact parameter representation, and contrast it with that of the π .

The pseudoscalar octet meson couplings to the nu-

cleon, as determined by $SU(3)$ flavor symmetry, and the definition of their impact parameter-dependent momentum distributions are summarized in Appendix A. Significant contributions come only from the $K\Lambda$ and $K\Sigma^*$ channels. The large- b behavior of these distributions is formally governed by the asymptotic expression, Eqs. (22) and (23), with the π mass replaced by the K mass. Figure 6 shows the numerically computed effective momentum distribution of K in $K\Lambda$ configurations, with and without restriction to large b , *cf.* Eq. (37), which should be compared to the corresponding distributions for the π in Fig. 5. One sees that the overall magnitude of $f_{K\Lambda}$ is substantially smaller than that of $f_{\pi N}$, because of the smaller coupling constant (no isospin degeneracy, *cf.* Appendix A) and the larger meson and intermediate baryon mass. More importantly, one notes that the restriction to large b suppresses the K distribution much more strongly than the π distribution; only about 1/5 of all kaons in the meson cloud model are located at transverse distances $b > 0.55 \text{ fm}$, and less than 1% are found at $b > 1.1 \text{ fm}$. While hardly surprising, these numbers show clearly that the K (and η) contribution to the partonic structure above the nucleon's core radius, $R_{\text{core}} = 0.55 \text{ fm}$ is extremely small.

IV. LARGE-DISTANCE COMPONENT OF THE NUCLEON SEA

A. Isovector sea $\bar{d} - \bar{u}$

We now apply the formalism developed in Secs. II and III to study the chiral large-distance contributions to the sea quark distributions in the nucleon. To this end, we evaluate the convolution formulas, Eqs. (27)–(28), with the b -integrated pion distribution, Eq. (37), where the lower limit, b_0 , is taken sufficiently large to exclude the model-dependent small-distance region, *cf.* Fig. 3. Our standard value for this parameter is the phenomenological “core” radius, Eq. (4); variation of this value will allow us to estimate the sensitivity of the results to unknown short-distance dynamics. While not permitting a complete description of the sea quark distributions, our results allow us to quantify how much comes from the “universal” large-distance region, providing guidance for future comprehensive models of the partonic structure.

We first consider the isovector antiquark distribution in the proton, $[\bar{d} - \bar{u}](x)$, which experiences only non-singlet QCD evolution and is largely independent of the normalization scale. The convolution formula Eq. (28) involves the valence quark distribution of the pion; the normalization of this distribution is fixed by Eq. (32), and its shape has been determined accurately by fits to the πN Drell–Yan data; see Ref. [36] and references therein. We use the leading-order parametrization of the valence distribution provided in Ref. [36]; the differences to the next-to-leading order parametrization are minor in this case. Figure 7 shows the chiral long-distance contribu-

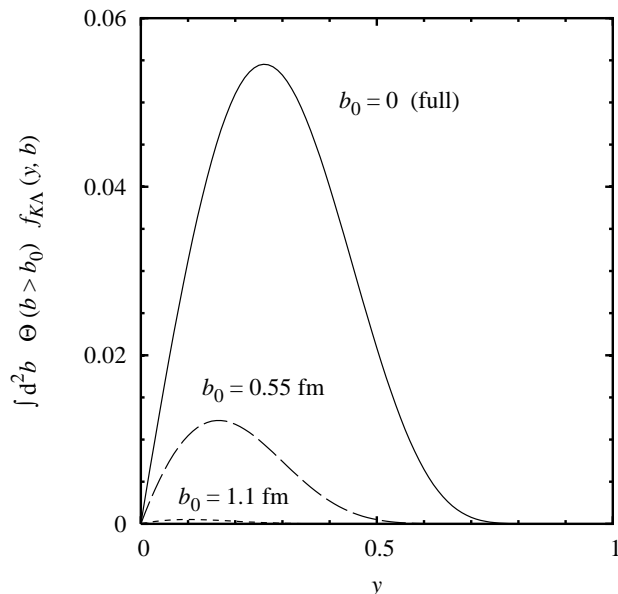


FIG. 6: Effective momentum distribution of kaons in $K\Lambda$ configurations with impact parameters $b > b_0$, *cf.* Eq. (37), in the meson cloud model with virtuality cutoff (exponential form factor, $\Lambda_{\text{virt}} = 1.0 \text{ GeV}$). *Solid line:* $b_0 = 0$ (full integral). *Dashed lines:* $b_0 = 0.55 \text{ fm}$ and $b_0 = 1.1 \text{ fm}$.

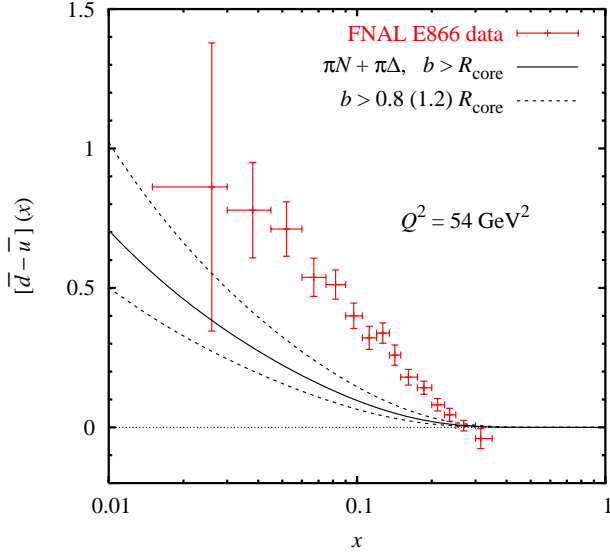


FIG. 7: *Solid line*: Large-distance contribution to the anti-quark flavor asymmetry, $[\bar{d} - \bar{u}](x)$, obtained from πN and $\pi\Delta$ configurations restricted to impact parameters $b > R_{\text{core}} = 0.55$ fm, cf. Eq. (37). *Dotted lines*: Same with $b > 0.8 R_{\text{core}}$ (upper line) and $1.2 R_{\text{core}}$ (lower line). *Data*: Result of analysis of final FNAL E866 Drell-Yan data [5]; statistical and systematic errors were added in quadrature. All curves and data points refer to the scale $Q^2 = 54 \text{ GeV}^2$.

tion obtained when b_0 is taken to be the phenomenological “core” radius, $R_{\text{core}} = 0.55$ fm (solid line), as well as the band covered when b_0 is changed from this value by $\pm 20\%$ (dotted lines). Also shown in the figure are the results of an analysis of the final data from the FNAL E866 Drell-Yan experiment, presented at a common scale $Q^2 = 54 \text{ GeV}^2$ [5]. One sees that the large-distance contribution to the asymmetry is practically zero for $x > 0.3$, as expected from the general considerations of Sec. II. At $x \sim 0.1$ the large-distance contribution accounts for $\sim 30\%$ of the measured asymmetry, indicating that most of it results from the nucleon’s core at small transverse distances. This conclusion is robust and, as demonstrated in Sec. III, does not depend on the form factors employed in the calculation within the pion cloud model (the specific results shown here were obtained with an exponential virtuality cutoff with $\Lambda_{\pi N} = 1.0 \text{ GeV}$ and $\Lambda_{\pi\Delta} = 0.8 \text{ GeV}$ [10]). At small x (~ 0.01) the large-distance contribution obtained in our approach comes closer to the data; however, the quality of the present data is rather poor, and it is difficult to infer the magnitude of the required “core” contribution by comparing the present estimate of the large-distance contribution to the data in this region of x .

One sees from Eq. (28) that the isovector antiquark distribution involves strong cancellations between the contributions from πN and $\pi\Delta$ intermediate states. This is not accidental — the cancellation between the two becomes exact in the large- N_c limit of QCD, and is in fact

necessary to restore the proper N_c scaling of the isovector distribution; see Sec. VI.

B. Isoscalar sea $\bar{u} + \bar{d}$

The isoscalar light antiquark distribution, $[\bar{u} + \bar{d}](x)$, is subject to singlet QCD evolution and thus exhibits stronger scale dependence than the isovector distribution. The convolution formula for this distribution, Eq. (27), involves the total (singlet) antiquark distribution in the pion, which we may write in the form

$$q_{\pi}^{\text{tot}}(z) = q_{\pi}^{\text{val}}(z) + 2q_{\pi}^{\text{sea}}(z), \quad (38)$$

where q_{π}^{val} is the valence distribution, Eq. (31), and q_{π}^{sea} the “sea” distribution [67]

$$q_{\pi}^{\text{sea}} = \bar{u}_{\pi+} = d_{\pi+} = u_{\pi-} = \bar{d}_{\pi-}. \quad (39)$$

The pion sea was determined within a radiative parton model analysis, supplemented by a constituent quark picture which relates the pion to nucleon parton densities, and found to be relatively small [36]. Again, we use the leading-order parametrization for the parton densities in the pion.

Figure 8 shows our result for the chiral large-distance contribution to the isoscalar antiquark distribution, separately for the valence and sea distributions in the pion as well as the total, at the scale $Q^2 = 2 \text{ GeV}^2$. One sees that the sea in the pion becomes important only at $x \ll M_{\pi}/M_N$, where the antiquark momentum fraction

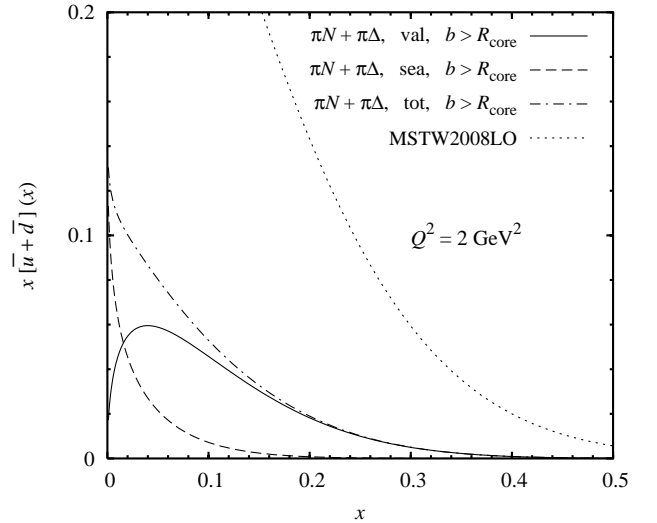


FIG. 8: *Solid/dashed/dashed-dotted line*: Large-distance contribution to the isoscalar antiquark density, $x[\bar{u} + \bar{d}]$, resulting from πN and $\pi\Delta$ configurations restricted to $b > R_{\text{core}} = 0.55$ fm. The plot shows separately the contributions arising from the valence, sea, and total antiquark density in the pion, cf. Eq. (38). *Dotted line*: MSTW2008LO leading-order parametrization [37].

in the pion can become small, $z \ll 1$. Altogether, the large-distance contribution accounts for only $\sim 1/5$ of the total $\bar{u} + \bar{d}$ in the nucleon at $x \sim 0.1$.

The antiquark distribution obtained from πB ($B = N, \Delta$) configurations cannot be larger than the total antiquark distribution in the nucleon, which includes the radiatively generated sea. The large-distance contribution calculated in our approach easily satisfies this theoretical constraint, as can be seen from the comparison with the parametrization obtained in the recent leading-order global fit of Ref. [37] (MSTW2008LO), see Fig. 8. We note that the traditional pion cloud model without restriction to large b , which generates pions with transverse momenta of the order ~ 1 GeV and virtualities ~ 1 GeV², produces an isoscalar sea which comes close to saturating the empirical $\bar{u} + \bar{d}$ at large x with the usual range of parameters, and can even overshoot it for certain choices [10, 35]. The restriction of πB configurations to large b in our approach solves this problem in a most natural way.

C. Strange sea s, \bar{s}

The strange sea (s, \bar{s}) in the nucleon at large distances has two distinct components. One is the chiral component, arising from s and \bar{s} in the pion in πN and $\pi \Delta$ configurations. It is given by a similar convolution formula as the isoscalar sea, $\bar{u} + \bar{d}$, Eq. (27),

$$\bar{s}(x, b)_{\text{chiral}} = \int_x^1 \frac{dy}{y} [f_{\pi N} + f_{\pi \Delta}](y, b) \bar{s}_\pi(z), \quad (40)$$

and similarly for s , where $\bar{s}_\pi(z)$ and $s_\pi(z)$ are the strange (anti-) quark distributions in the pion. Assuming that the sea in the pion is mostly generated radiatively [36], we take them to be equal and proportional to the non-strange sea in the pion, Eq. (39),

$$\bar{s}_\pi(z) = s_\pi(z) = q_\pi^{\text{sea}}(z). \quad (41)$$

The other component comes from valence \bar{s} quarks in KY ($Y = \Lambda, \Sigma, \Sigma^*$) and ηN configurations in the nucleon. Because the masses of these mesons are numerically comparable to the typical hadronic mass scale (as given, say, by the vector meson mass), their contribution to the partonic structure of the nucleon cannot strictly be associated with chiral dynamics, even at large transverse distances. We include them in our numerical studies because (a) it is instructive to contrast their contribution to those of πN and $\pi \Delta$; (b) they contribute to \bar{s} only and could in principle generate different x -distributions for s and \bar{s} , as suggested by the model of Ref. [38] (we shall comment on this model below). The couplings of the octet mesons to the nucleon, as determined by $SU(3)$ symmetry and the quark model value of the F/D ratio, as well as the definitions of the corresponding meson momentum distributions are summarized in Appendix A.

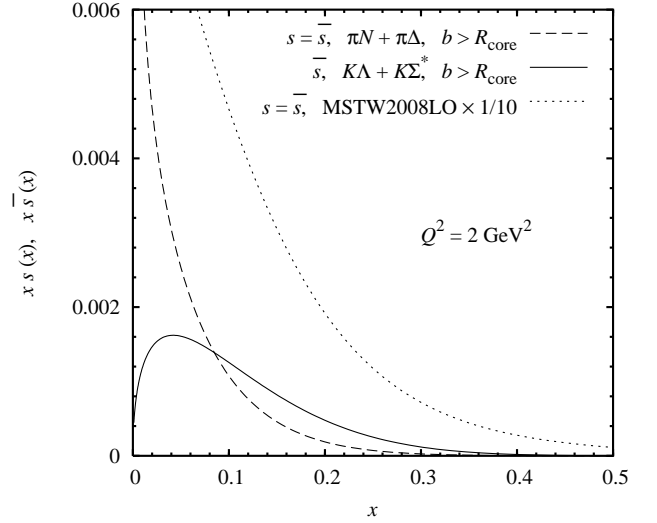


FIG. 9: *Dashed line*: Large-distance contribution to the strange sea in the nucleon, $s = \bar{s}$, from πN and $\pi \Delta$ configurations ($b > R_{\text{core}} = 0.55$ fm). *Solid line*: Large-distance contribution to \bar{s} from $K\Lambda$ and $K\Sigma^*$ configurations, involving the valence strange quark distribution in the kaon; $K\Sigma$ and ηN are numerically negligible. *Dotted line*: MSTW2008LO leading-order parametrization of the total $s = \bar{s}$ [37], multiplied by 1/10 for easier comparison.

The contribution of K and η to $\bar{s}(x, b)$ in the proton is obtained as

$$\begin{aligned} \bar{s}(x, b) = & \int_x^1 \frac{dy}{y} \left\{ \frac{2}{3} f_{\eta N}(y, b) \bar{s}_\eta(z) \right. \\ & \left. + [f_{K\Lambda} + f_{K\Sigma} + f_{K\Sigma^*}](y, b) \bar{s}_K(z) \right\}, \quad (42) \end{aligned}$$

where the factor $2/3$ accounts for the probability of the η to be in a configuration with a valence \bar{s} quark (we assume a pure octet state of the η and do not take into account singlet-octet mixing, as the η contribution turns out to be negligibly small anyway). The functions $\bar{s}_\eta(z)$ and $\bar{s}_K(z)$ are the normalized momentum distributions of \bar{s} in η and K ,

$$\int_0^1 dz \bar{s}_{\eta, K}(z) = 1. \quad (43)$$

Assuming $SU(3)$ symmetry, we will approximate these distributions by the valence quark distribution in the pion,

$$\bar{s}_{\eta, K}(z) \approx q_\pi^{\text{val}}(z). \quad (44)$$

We again use the leading-order parametrization of Ref. [36] for the valence quark density in the pion. Numerical evaluation of the meson distributions shows that the contributions from ηN and $K\Sigma$ in Eq. (42) are negligible because of their relatively small coupling; we retain only the $K\Lambda$ and $K\Sigma^*$ terms in the following.

Figure 9 shows the different large-distance contributions to the strange sea, integrated over $b > R_{\text{core}} =$

0.55 fm. One sees that for $x > 0.1$ the large-distance strange sea is mostly \bar{s} coming from the valence \bar{s} in $K\Lambda$ and $K\Sigma^*$ configurations; the precise magnitude of this contribution is sensitive to the lower limit in b , cf. Fig. 6. For $x < 0.1$ the large-distance strange sea in the nucleon originates mostly from the strange sea in the pion in πB ($B = N, \Delta$) configurations, which contributes equally to s and \bar{s} . The different mechanisms result in $s(x) \neq \bar{s}(x)$ for the large-distance component of the strange sea. However, the overall magnitude of the large-distance component represents only $\sim 1/20$ of the empirically determined average strange sea, $\frac{1}{2}[s + \bar{s}](x)$ [37], so that one cannot draw any conclusions about the x -distributions of the total s and \bar{s} in the nucleon from the large-distance component. Note that the large-distance component at $b > R_{\text{core}}$ represents a much smaller fraction of the total sea in the case of s and \bar{s} than for $\bar{u} + \bar{d}$, at least in the region $x \gtrsim 0.01$.

There are significant differences between the leading-order parametrizations of $[s + \bar{s}](x)$ obtained in the global fits of Refs. [37] and [39]; up to a factor ~ 2 at $x = 0.1$. However, this does not change our basic conclusion, that the large-distance s and \bar{s} are only a small fraction of the total. Also, some of the next-to-leading order fits by several groups [37, 40] have begun to extract information on the shapes of $s(x)$ and $\bar{s}(x)$ individually, by incorporating neutrino scattering data which discriminate between the two. The difference $[s - \bar{s}](x)$ is very poorly determined by the existing data, and the fits serve mostly to limit the range of allowed values. We note that our approach to large-distance contributions and the convolution formulas of Eqs. (26)–(28) remain valid also for next-to-leading order parton densities, if the parton densities in the pion are taken to be the next-to-leading order ones. In the present study we restrict ourselves to the leading order, because at this order the parton densities are renormalization-scheme-independent and possess a simple probabilistic interpretation, and because the present comparison of our results with the data does not warrant high accuracy.

We would like to comment on the approach of Ref. [38], where the shapes of $s(x)$ and $\bar{s}(x)$ were investigated in a light-front wave function model with $K\Lambda$ components, whose amplitude was adjusted to fit the observed total strange sea, $[s + \bar{s}](x)$. As just explained, our results show that only a very small fraction of the total s and \bar{s} sea arise from transverse distances $b > R_{\text{core}} \approx 0.55$ fm where the notion of meson-baryon components in the nucleon wave function is physically sensible. Even in the traditional meson cloud model without restriction to large b , $K\Lambda$ configurations with standard form factors [10, 41] would account only for $\sim 1/4$ of the present value of $s + \bar{s}$ [37]. This shows that the assumption of saturation of the strange sea by $K\Lambda$ configurations made in Ref. [38] would require a $K\Lambda$ coupling ~ 2 times larger than the $SU(3)$ value and is not realistic. While we see indications for $s(x) \neq \bar{s}(x)$ in the large-distance contribution, and certainly nothing requires the shapes to be equal,

the magnitude of the effect cannot be reliably predicted on the basis of the model of Ref. [38].

D. Flavor asymmetry $\bar{u} + \bar{d} - 2\bar{s}$

The antiquark $SU(3)$ flavor asymmetry $\bar{u} + \bar{d} - 2\bar{s}$ is a non-singlet combination of the isoscalar non-strange and strange sea, which exhibits only weak scale dependence. Since we assume $SU(3)$ flavor symmetry of the sea quarks in the pion, Eq. (41), only the valence π and K components of $\bar{u} + \bar{d}$ and \bar{s} enter in this combination (we neglect the ηN and $K\Sigma$ contributions):

$$[\bar{u} + \bar{d} - 2\bar{s}](x, b) \approx \int_x^1 \frac{dy}{y} [f_{\pi N} + f_{\pi \Delta} - 2f_{K\Lambda} - 2f_{K\Sigma^*}](y, b) \bar{q}_{\pi}^{\text{val}}(z). \quad (45)$$

The large-distance contribution to this asymmetry is shown in Fig. 10. One sees that the asymmetry overwhelmingly results from the valence \bar{u} and \bar{d} content of the pion in πN and $\pi \Delta$ configuration; the \bar{s} in the kaon of $K\Lambda$ and $K\Sigma^*$ contributes only at the level of $< 10\%$ of the pion. Overall, the large-distance contribution accounts for $\sim 1/3$ of the observed $SU(3)$ flavor asymmetry at $x \sim 0.1$.

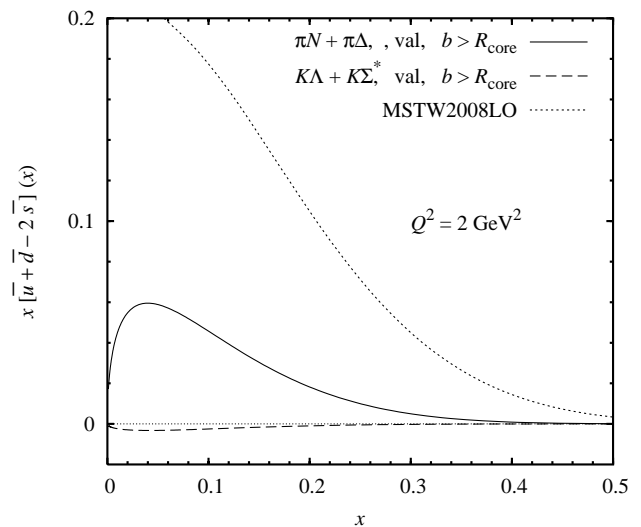


FIG. 10: *Solid line*: Large-distance contribution to the antiquark $SU(3)$ flavor asymmetry in the nucleon $\bar{u} + \bar{d} - 2\bar{s}$ from valence $\bar{u} + \bar{d}$ in the pion in πN and $\pi \Delta$ configurations, cf. Fig. 8 ($b > R_{\text{core}} = 0.55$ fm). *Dashed line*: Contribution from the valence \bar{s} in the kaon in $K\Lambda$ and $K\Sigma^*$ configurations, cf. Fig. 9. *Dotted line*: Leading-order parametrization of Ref. [37].

V. TRANSVERSE SIZE OF NUCLEON

A. Transverse size and GPDs

An interesting characteristic of the nucleon's partonic structure is the average squared transverse radius of the partons with given longitudinal momentum fraction x . It is defined as

$$\langle b^2 \rangle_f(x) \equiv \frac{\int d^2b b^2 f(x, b)}{f(x)} \quad (f = q, \bar{q}, g), \quad (46)$$

where $f(x, b)$ is the impact parameter-dependent distribution of partons, related to the total parton density by

$$\int d^2b f(x, b) = f(x). \quad (47)$$

The average is meaningful thanks to the positivity of $f(x, b)$ [12, 13]. Physically, Eq. (46) measures the average transverse size of configurations in the nucleon wave function contributing to the parton density at given x . The transverse size implicitly depends also on the scale, Q^2 ; this dependence arises from the DGLAP evolution of the impact-parameter dependent parton distribution and was studied in Ref. [42].

The average transverse quark/antiquark/gluon size of the nucleon is directly related to the t -slope of the corresponding nucleon GPD at $t = 0$,

$$\langle b^2 \rangle_f(x) = 4 \frac{\partial}{\partial t} \left[\frac{H_f(x, t)}{H_f(x, 0)} \right]_{t=0}. \quad (48)$$

Here $H_f(x, t) \equiv H_f(x, \xi = 0, t)$ denotes the “diagonal” GPD (zero skewness, $\xi = 0$), with $H_f(x, 0) = f(x)$, which is related to the impact parameter-dependent distribution as ($b \equiv |\mathbf{b}|$)

$$H_f(x, t = -\Delta_\perp^2) = \int d^2b e^{-i(\Delta_\perp \cdot \mathbf{b})} f(x, b). \quad (49)$$

For a general review of GPDs and their properties we refer to Refs.[43].

B. Transverse size from hard exclusive processes

By virtue of its connection with the GPDs, the transverse size of the nucleon is in principle accessible experimentally, through the t -slope of hard exclusive processes,

$$\gamma^*(Q^2) + N \rightarrow M + N \quad (M = \text{meson}, \gamma, \dots),$$

at $Q^2 \gg 1 \text{ GeV}^2$ and $|t| \lesssim 1 \text{ GeV}^2$, whose amplitude can be calculated using QCD factorization and is proportional to the nucleon GPDs. In general, such processes require a longitudinal momentum transfer to the nucleon and probe the “non-diagonal” GPDs ($\xi \neq 0$), so that the connection between the observable t -slope and the

transverse size can be established only with the help of a GPD parametrization which relates the distributions at $\xi \neq 0$ to those at $\xi = 0$. The connection becomes simple in the limit of high-energy scattering, $\xi \approx x_B/2 \ll 1$, where the GPDs probed in the hard exclusive process can be related to the diagonal ones in a well-controlled approximation; see Refs. [44, 45] for details. In this approximation the amplitudes for light vector meson electroproduction at small x (ϕ, ρ) and heavy vector meson photo/electroproduction ($J/\psi, \Upsilon$) are proportional to the diagonal gluon GPD, and thus

$$(d\sigma/dt)^{\gamma^* N \rightarrow V+N} \propto H_g^2(x = x_B, t). \quad (50)$$

The gluonic average transverse size can be directly inferred from the relative t -dependence of the differential cross section

$$\langle b^2 \rangle_g = 4 \frac{\partial}{\partial t} \left[\frac{d\sigma/dt(t)}{d\sigma/dt(0)} \right]_{t=0}^{1/2}. \quad (51)$$

The universal t -dependence of exclusive ρ^0 and ϕ electroproduction at sufficiently large Q^2 and exclusive J/ψ photo/electroproduction, implied by Eq. (50), is indeed observed experimentally and represents an important test of the approach to the hard reaction mechanism; see Ref. [46] for a recent compilation of results.

Experimental information on the nucleon's gluonic size and its dependence on x comes mainly from the extensive data on the t -dependence of exclusive J/ψ photo/electroproduction, measured in the HERA H1 [15] and ZEUS [16] experiments, as well as the FNAL E401/E458 [17] and other fixed-target experiments; see Ref. [47] for a recent summary. The t -dependence of the cross section measured in the HERA experiments is well described by an exponential,

$$(d\sigma/dt)^{\gamma N \rightarrow J/\psi+N} \propto \exp(B_{J/\psi} t), \quad (52)$$

and assuming that this form is valid near $t = 0$, the nucleon's average gluonic transverse size is obtained as

$$\langle b^2 \rangle_g = 2B_{J/\psi}. \quad (53)$$

For a more accurate estimate, the measured t -slope is reduced by $\sim 0.3 \text{ GeV}^{-2}$ to account for the finite size of the produced J/ψ . The exponential slope measured by H1 at $\langle W \rangle = 90 \text{ GeV}$ is $B_{J/\psi} = 4.630 \pm 0.060^{+0.043}_{-0.163} \text{ GeV}^{-2}$ [15], and ZEUS quotes a value of $B_{J/\psi} = 4.15 \pm 0.05^{+0.30}_{-0.18} \text{ GeV}^{-2}$ [16]. The central values correspond to a transverse gluonic size at $x \sim 10^{-3}$ in the range $\langle b^2 \rangle_g = 0.31 - 0.35 \text{ fm}^2$, substantially smaller than the transverse size of the nucleon in soft hadronic interactions. It is also found that the gluonic size increases with $\log(1/x)$ with a coefficient much smaller than the soft-interaction Regge slope, *cf.* the discussion in Sec. VII A.

Comparatively little is known about the quark size of the nucleon at small x . As explained above, light vector meson production at small x couples mainly to

the gluon GPD. Interesting new information comes from the t -dependence of deeply-virtual Compton scattering (DVCS) recently measured at HERA. The H1 experiment [19] obtained an exponential slope of $B_\gamma = 5.45 \pm 0.19 \pm 0.34 \text{ GeV}^{-2}$ by measuring t through the photon transverse momentum; larger by one unit than the J/ψ slope measured by the same experiment. ZEUS [20] extracted a DVCS slope of $B_\gamma = 4.5 \pm 1.3 \pm 0.4 \text{ GeV}^{-2}$ by measuring the transverse momentum of the recoiling proton, again larger than the J/ψ slope measured by that experiment; however, the exponential fit to the ZEUS data is rather poor and the extracted B_γ has large errors. We note that in both experiments the B_γ values were determined by an exponential fit over the entire measured region of t and thus reflect the average t -dependence, not directly the slope at $t = 0$. Still, the data provide some indication that the t -slope of DVCS at $t = 0$ is larger than that of J/ψ production (the Q^2 in the DVCS experiments here are comparable to the effective scale in J/ψ photoproduction, $Q_{\text{eff}}^2 \approx 3 \text{ GeV}^2$). In leading-order (LO) QCD factorization, the DVCS amplitude is proportional to the singlet quark GPDs, and the t -slope of this process is directly related to the nucleon's singlet quark size,

$$\langle b^2 \rangle_{q+\bar{q}} = 2B_\gamma, \quad (54)$$

cf. Eq. (53). One would thus conclude that

$$\langle b^2 \rangle_{q+\bar{q}} > \langle b^2 \rangle_g. \quad (55)$$

At next-to-leading order (NLO) the DVCS amplitude also involves the gluon GPD, and substantial cancellation is found between the gluon and singlet quark contributions to the amplitude. This cancellation amplifies the effect of a difference in $\langle b^2 \rangle_{q+\bar{q}}$ and $\langle b^2 \rangle_g$ on the DVCS t -slope. Because the gluon contribution is negative and cancels $\sim 1/2$ of the quark contribution [48], the relative change in the slope should be ~ 2 times larger than the relative change in the average transverse sizes which caused it [49].

The quark transverse size of the nucleon in the valence quark region is measured in hard exclusive processes at Jefferson Lab, in particular with the 12 GeV Upgrade. In this kinematics the skewness of the GPDs needs to be taken into account ($\xi \neq 0$), and the analysis relies on GPD parametrizations. It is interesting that the t -slope of ρ^0 production measured in the recent CLAS experiment [50] seems to be compatible with the Regge-based GPD parametrization of Ref. [51] (however, it is presently unclear how to describe the absolute cross section within this framework). A detailed phenomenological study of the transverse distribution of valence quarks, based on parton densities and form factor data, was performed in Ref. [52].

C. Chiral contribution

We now want to study the contribution of the chiral large-distance region, $b \sim 1/M_\pi$, to the nucleon's average transverse size. Adopting a two-component description, we define

$$\begin{aligned} \langle b^2 \rangle_f &= \frac{\int d^2b b^2 [f(x, b)_{\text{core}} + \Theta(b > b_0) f(x, b)_{\text{chiral}}]}{f(x)} \\ &\equiv \langle b^2 \rangle_{f, \text{core}} + \langle b^2 \rangle_{f, \text{chiral}}. \end{aligned} \quad (56)$$

Here $f(x, b)_{\text{core}}$ denotes the parton density arising from average configurations in the nucleon, distributed over transverse distances $b \sim R_{\text{core}}$. The function $f(x, b)_{\text{chiral}}$ is the chiral component of the parton distribution, extending over distances $b \sim 1/M_\pi$. Following the same approach as above, we integrate it over b with a lower cutoff, b_0 , of the order of the core radius, Eq. (4); the sensitivity of the results to the precise value of b_0 will be investigated below. Note that in Eq. (56) the b^2 -weighted integral in the numerator is computed in two separate pieces, while the denominator in both cases is the total parton density (core plus chiral) at the given value of x ; the $\langle b^2 \rangle_{f, \text{chiral}}$ thus defined represents the contribution of the chiral component to the overall transverse size of the nucleon, not the “intrinsic” size of the chiral component alone.

The “core” contribution to $\langle b^2 \rangle$ was estimated in Sec. II A and Ref. [14], by relating it to the slope of the nucleon's axial form factor, which does not receive contributions from the pion cloud:

$$\langle b^2 \rangle_{\text{core}} \approx \frac{2}{3} \langle r^2 \rangle_{\text{axial}} = 0.3 \text{ fm}^2. \quad (57)$$

We have already used this result to fix the short-distance cutoff in the integral over the chiral contribution. A more quantitative determination of the “non-chiral” transverse sizes of the nucleon, including the differences between quarks, antiquarks and gluons and their x -dependence, requires a dynamical model of the nucleon which smoothly interpolates between small and large distances and will be the subject of a separate study. Here we focus on the chiral contribution, $\langle b^2 \rangle_{f, \text{chiral}}$, which can be calculated in a model-independent manner; we compare it to the “generic” core size given by Eq. (57), keeping in mind that the latter may have a richer structure than reflected by this simple estimate.

The chiral contribution to the transverse size, Eq. (56), is obtained by calculating the b^2 -weighted integral of the b -dependent pion momentum distribution in the nucleon studied in Sec. III, *cf.* Eq. (37), and substituting the result in the convolution formula for the nucleon parton density, Eq. (27) *et seq.* Useful formulas for the numerical evaluation of the b^2 -weighted integrals are presented in Appendix B. Because of the weighting factor b^2 , the chiral contribution to the transverse size is much less sensitive to unknown short-distance dynamics (*i.e.*, to the cutoff b_0) than the contribution to the parton density

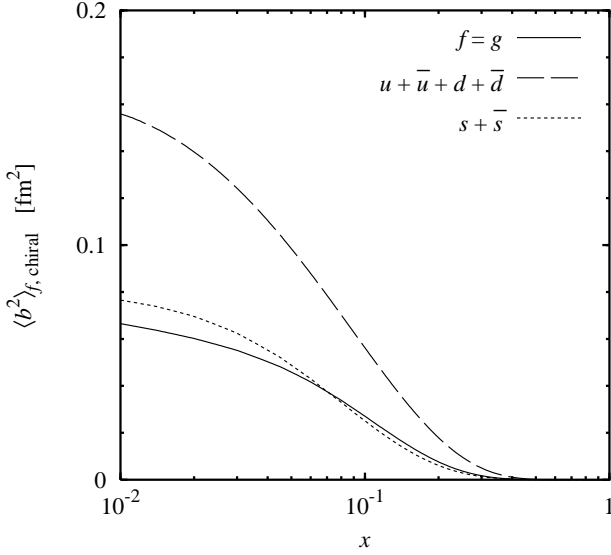


FIG. 11: The chiral large-distance contribution to the nucleon's average transverse size, $\langle b^2 \rangle_f$, as defined by Eq. (56), as a function of x ($Q^2 = 3 \text{ GeV}^2$). Solid line: Gluonic size ($f = g$), cf. Ref. [14]. Dashed line: Singlet quark size ($f = u + \bar{u} + d + \bar{d}$). Dotted line: Strange quark size ($f = s + \bar{s}$). In all cases, the curves show the sum of contributions from πN and $\pi \Delta$ configurations.

itself, and thus represents a much more interesting quantity for studying effects of chiral dynamics in the partonic structure. Furthermore, the b^2 -weighted integral can reliably be computed using the asymptotic form of the distribution of pions at large b , Eq. (22), as was done in Ref. [14]. We can use this to estimate analytically the sensitivity of $\langle b^2 \rangle_{f, \text{chiral}}$ to the lower limit, b_0 . Evaluating the integral

$$I \equiv \int d^2b \Theta(b > b_0) b^2 f_{\pi N}(y, b) \quad (58)$$

with the asymptotic expression Eq. (22), and taking the logarithmic derivative with respect to b_0 , we obtain

$$-\frac{b_0}{I} \frac{\partial I}{\partial b_0} \approx \frac{1}{5} \ll 1 \quad (y = M_\pi/M_N), \quad (59)$$

where we have used Eq. (25) for κ_N and $b_0 = R_{\text{core}} = 0.55 \text{ fm}$. This shows that the sensitivity of $\langle b^2 \rangle_{\text{chiral}}$ is indeed low — a 20% change in b_0 causes only a 4% change in $\langle b^2 \rangle_{f, \text{chiral}}$.

Our results for the chiral contribution to the nucleon's average transverse size and its dependence on x are summarized in Fig. 11, for the scale $Q^2 = 3 \text{ GeV}^2$. The curves shown are the sum of contributions from πN and $\pi \Delta$ configurations; heavier mesons make negligible contributions at large distances. For reasons of consistency the nucleon parton densities in the denominator of Eq. (56) were evaluated using the older parametrization of Ref. [53], which served as input to the analysis of the pion parton distributions of Ref. [36]. The following features are worth mentioning:

- (a) The chiral contribution to the transverse size is practically zero above $x \sim M_\pi/M_N \sim 0.1$ and grows rapidly as x drops below this value, in agreement with the basic picture described in Sec. II. The rise of $\langle b^2 \rangle_{f, \text{chiral}}$ with decreasing x is more pronounced than that of the parton density itself because the former quantity emphasizes the contributions from large distances.
- (b) The singlet u - and d -quark size grows more rapidly with decreasing x than the gluonic radius. This has a simple explanation: the quark/antiquark density in the pion sits at relatively large momentum fractions $z \sim 0.5$, while the gluon density in the pion requires $z < 0.1$ to be sizable; because $z = x/y$ in the convolution integral, and the pion momentum fractions are of the order $y \sim M_\pi/M_N$, the relevant values of z are reached much earlier for the quark than for the gluon as x decreases below M_π/M_N . Thus, the chiral large-distance contribution suggests that the transverse quark size of the nucleon at $x \lesssim 0.01$ is larger than the transverse gluon size, cf. Eq. (55). The difference between the chiral contribution to the average sizes at $x = 0.01$ is

$$\langle b^2 \rangle_{q+\bar{q}, \text{chiral}} - \langle b^2 \rangle_{g, \text{chiral}} = 0.09 \text{ fm}^2. \quad (60)$$

Assuming identical core sizes for the quark and gluon distribution, this would correspond to a difference of the leading-order DVCS and J/ψ t -slopes, cf. Eqs. (53) and (54),

$$B_\gamma - B_{J/\psi} = 1.1 \text{ GeV}^2, \quad (61)$$

well consistent with the HERA results summarized in Sec. VB. It should be remembered that the chiral prediction, Eq. (61), is for the exact t -slope of the cross section at $t = 0$, while the HERA results represent effective slopes, obtained by fitting the empirical t -dependence over the measured range; the comparison may be affected by possible deviations of the true t -dependence from the exponential shape. More quantitative conclusions would require detailed modeling of the core contributions to the transverse size, which themselves can grow with decreasing x due to diffusion, see Sec. VII A.

- (c) The chiral contribution to the transverse strange quark size of the nucleon closely follows that to the gluonic size. This is natural, as $s + \bar{s}$ is mostly generated radiatively, by conversion of gluons into $s\bar{s}$, in both the pion and the nucleon.

VI. PION CLOUD AND LARGE- N_c QCD

The relation of the chiral component of the large- b parton densities to the large- N_c limit of QCD is a problem of both principal and practical significance. First, in the

large- N_c limit QCD is expected to become equivalent to an effective theory of mesons, in which baryons appear as solitonic excitations, establishing a connection with the phenomenological notion of meson exchange. Second, our calculations show that contributions from Δ intermediate states are numerically large, and the large- N_c limit provides a conceptual framework which allows one to treat N and Δ states on the same footing and relate their masses and coupling constants. We now want to verify that the large-distance component of the nucleon's partonic structure, calculated from phenomenological pion exchange, exhibits the correct N_c -scaling required of parton densities in QCD (*cf.* also the discussion in Ref. [14]).

The general N_c scaling of the unpolarized quark densities in the nucleon in QCD is of the form [54]

$$g(x) \sim N_c^2 \times \text{function}(N_c x), \quad (62)$$

$$[u + d](x), [\bar{u} + \bar{d}](x) \sim N_c^2 \times \text{function}(N_c x), \quad (63)$$

$$[u - d](x), [\bar{u} - \bar{d}](x) \sim N_c \times \text{function}(N_c x), \quad (64)$$

where the scaling functions are stable in the large- N_c limit but can be different between the various distributions. Equations (63) and (64) were derived by assuming non-exceptional configurations ($x \sim N_c^{-1}$) and fixing the normalization of the scaling function from the lowest moments of the parton densities, *i.e.*, from the conditions that the total number of quarks scale as N_c , and the nucleon isospin as N_c^0 . The transverse coordinate-dependent parton distributions should generally scale in the same manner as the total densities, Eqs. (63) and (64), as the nucleon radius is stable in the large- N_c limit (this applies even to the nucleon's chiral radii, because $M_\pi \sim N_c^0$).

Turning now to the pion cloud contribution to the parton densities at large b , it follows from the expressions of Eqs. (14)–(18) and their Fourier transform, Eq. (8), that the b -dependent distributions of pions in the nucleon scale as [14]

$$f_{\pi N}(y, b), f_{\pi \Delta}(y, b) \sim N_c^2 \times \text{function}(N_c x). \quad (65)$$

This behavior applies to values $y \sim M_\pi/M_N \sim N_c^{-1}$ and values $b \sim N_c^0$, corresponding to $|t| \sim N_c^0$ in the pion GPD. In arriving at Eq. (65) we have used that $M_N, M_\Delta \sim N_c$; that $g_{\pi NN} \sim N_c^{3/2}$, as implied by the Goldberger-Treiman relation; and that $g_{\pi N \Delta}$ scales in the same way as $g_{\pi NN}$. Equation (65) states that the momentum distribution of pions in the nucleon at large N_c scales like that of isoscalar quarks or gluons. At the same time, the parton densities in the pion scale as

$$g_\pi(z), q_\pi(z) \sim \text{function}(z), \quad (66)$$

where $z \sim N_c^0$ in typical configurations; that is, they have no explicit N_c dependence at large N_c . One thus concludes that the N_c -scaling of the convolution integral for the pion cloud contribution to the nucleon's antiquark densities, for both $B = N$ and Δ intermediate states, is

$$\int_x^1 \frac{dy}{y} f_{\pi B}(y, b) q_\pi(z) \sim N_c^2 \times \text{function}(N_c x). \quad (67)$$

This correctly reproduces the general N_c -scaling of the isoscalar quark and gluon distribution, Eq. (63), where the N and Δ contributions are added, *cf.* Eq. (28). However, it may seem that the pion cloud contribution at large b cannot reproduce the N_c scaling of the isovector distribution, Eq. (63), which is suppressed by one power. The paradox is resolved when one notes that in the large- N_c limit the N and Δ become degenerate,

$$M_\Delta - M_N \sim N_c^{-1}, \quad (68)$$

and their couplings are related by [55]

$$g_{\pi N \Delta} = \frac{3}{2} g_{\pi NN}. \quad (69)$$

Using these relations one has

$$f_{\pi \Delta}(y, b) = 2 f_{\pi N}(y, b) \quad (y \sim N_c^{-1}), \quad (70)$$

as can be seen from Eqs. (14)–(18) and Eq. (8), keeping in mind that $t, t_1, t_2 \sim N_c^0$ in the region of interest. By virtue of Eq. (70) the N and Δ contributions at large N_c cancel exactly in the isovector convolution integral, Eq. (64), ensuring that the result has the proper N_c -scaling behavior as Eq. (64).

In sum, our arguments show that the pion exchange contribution at large b is a legitimate part of the nucleon's partonic structure in large- N_c QCD, exhibiting the same scaling behavior as the corresponding “average” distributions. The inclusion of $\pi\Delta$ configurations at the same level as πN is essential because they reproduce the proper N_c -scaling of the isovector distributions, and because they make numerically sizable contributions — twice larger than πN — to the isoscalar distributions.

In Ref. [14] we have shown that the isoscalar large- b pion distribution in the nucleon $[f_{\pi N} + f_{\pi \Delta}](y, b)$ obtained from phenomenological soft-pion exchange, can equivalently be computed in the chiral soliton picture of the nucleon at large N_c , as a certain longitudinal Fourier transform of the universal classical pion field of the soliton at large transverse distances. Extending this connection to the isovector pion distribution, $[\frac{2}{3}f_{\pi N} - \frac{1}{3}f_{\pi \Delta}](y, b)$, which is suppressed in the large- N_c limit, remains an interesting problem for further study. In particular, this requires establishing the connection between soft-pion exchange and the collective rotations of the classical soliton.

VII. SMALL x -REGIME AND LONGITUDINAL DISTANCES

A. Growth of core size through diffusion

In our studies so far we have focused on chiral contributions to the nucleon's partonic structure at moderately small momentum fractions, $x \gtrsim 10^{-2}$, which arise from individual πB ($B = N, \Delta$) configurations in the nucleon

wave function. When considering smaller values of x several effects must be taken into account which potentially limit the validity of the present approximations.

One of them is the growth of the transverse size of “average” partonic configurations in the nucleon due to diffusion. Generally, the partons at small x are decay products of partons at larger x ; the decay process has the character of a random walk in transverse space and leads to a logarithmic growth of the transverse area occupied by the partons:

$$\langle b^2 \rangle_{\text{parton}} = \langle b^2 \rangle_{\text{parton}}(x_0) + 4\alpha'_{\text{parton}} \ln(x_0/x) \quad (x < x_0 \sim 10^{-2}). \quad (71)$$

The rate of growth — the effective Regge slope, α'_{parton} — depends on the type of parton and generally decreases with increasing scale Q^2 , because higher Q^2 increase the effective transverse momenta in the decay process [42]. Measurements of the energy dependence of the t -slope of exclusive J/ψ production at HERA H1 and ZEUS [15, 16] indicate that the rate of growth for gluons at a scale $Q^2 \approx 3 \text{ GeV}^2$ is approximately $\alpha'_g \approx 0.14 \text{ GeV}^{-2}$ [68] significantly smaller than the rate of growth of the transverse nucleon size in soft hadronic interactions, $\alpha'_{\text{soft}} \approx 0.25 \text{ GeV}^{-2}$. Using the former value as a general measure of the rate of growth of the nucleon’s transverse size due to diffusion, we estimate that at $Q^2 \approx 3 \text{ GeV}^2$ the transverse size of the “core” increases from $R_{\text{core}}^2 = 0.3 \text{ fm}^2$ at $x = 10^{-2}$ to $0.35 (0.4) \text{ fm}^2$ at $x = 10^{-3} (10^{-4})$. In principle this effect pushes the region of πB configurations governed by chiral dynamics out to larger b as x decreases. However, the rate of growth at this scale is still rather small, leaving ample room for such configurations in the region $x > 10^{-3}$. Note that at lower scales the rate of growth is larger; studies based on DGLAP evolution show that α'_g approaches the soft value at $Q^2 \sim 0.4 \text{ GeV}^2$ [42].

B. Chiral corrections to pion structure

Another effect which needs to be taken into account at small x are modifications of the parton density in the pion itself due to chiral dynamics. The same mechanism as discussed above for the nucleon in principle works also in the pion itself — the pion can fluctuate into configurations containing a “slow” pion and a two-pion spectator system. When evaluated in chiral perturbation theory, the momentum fraction of the slow pion relative to its parent in such configurations is of the order $y(\pi \text{ in } \pi) \sim M_\pi/(4\pi F_\pi)$, where F_π is the pion decay constant, and $4\pi F_\pi$ represents the generic short-distance scale appearing in the context of the renormalization of the loop integrals. Such contributions to the parton density and the GPD in the pion were recently computed in an all-order resummation of the leading logarithmic approximation to chiral perturbation theory [31], which does not require knowledge of the higher-order terms in

the chiral Lagrangian. For the nucleon parton densities this mechanism could become important for $x \ll 10^{-2}$, where the effective parton momentum fractions in the pion can reach small values $z \lesssim 0.1$. In the present study we restrict ourselves to nucleon parton densities at $x \gtrsim 10^{-2}$, for which the convolution integrals are dominated by “non-chiral” values of z . The incorporation of such corrections to the partonic structure of the pion and extension of the present nucleon structure calculation toward smaller x remains an interesting problem for future study. In particular, it should be investigated how the expressions derived in the leading-log approximation of chiral perturbation theory compare to a “single-step” calculation of pion structure including finite mass and size (form factors), along the lines done here for the nucleon.

C. Chiral dynamics at large longitudinal distances

In our studies in Secs. II–V we considered chiral contributions to the nucleon’s partonic structure at large transverse distances, which arise from πB configurations at large transverse separations, $b \sim 1/M_\pi$. As already indicated in Sec. II A, there is in principle another class of πB configurations governed by chiral dynamics, namely those corresponding to large longitudinal separations in the nucleon rest frame,

$$l \sim 1/M_\pi, \quad (72)$$

and arbitrary values of the transverse separation, down to $b = 0$. We now want to discuss in which region of x such configurations can produce distinct contributions to the partonic structure.

The main limitation in admitting πB configurations of the type Eq. (72) as part of the partonic structure arises from the possible longitudinal overlap of the relevant partonic configurations in the pion and the “core.” To determine the region where this effect plays a role, it is useful to consider instead of the parton densities the structure function for $\gamma^* N$ scattering and appeal to the notion of the coherence length of the virtual photon. Contributions to the partonic structure of the type of the convolution integrals of Eqs. (26)–(28) correspond to the impulse approximation of $\gamma^* N$ scattering, which requires that the coherence length of the process be smaller than the longitudinal distance between the constituents, so that interference effects can be neglected; see *e.g.* Ref. [56]. Generally, the coherence length for $\gamma^* N$ scattering in the nucleon rest frame is given by

$$l_{\text{coh}} = (2M_N x)^{-1}, \quad (73)$$

where M_N is the nucleon mass and $x \approx Q^2/W^2 \ll 1$ the Bjorken variable; W is the center-of-mass energy of the scattering process. Thus, one would naively think that in scattering from a πN system with longitudinal separation $\sim (2M_\pi)^{-1}$ coherence effects set in if $x <$

$M_\pi/M_N \sim 0.1$. However, this argument neglects the fact that in the fast-moving nucleon the pion carries only a fraction of the order $y \sim M_\pi/M_N \sim 0.1$ of the nucleon's momentum, so that the effective center-of-mass energy for $\gamma^*\pi$ scattering is actually lower by this factor, and the coherence length smaller by this factor, than in the γ^*N process. Interference effectively takes place only when the coherence length for both scattering on the pion and on the baryon in the πB configuration is $\sim (2M_\pi)^{-1}$, which requires

$$x \lesssim 0.01. \quad (74)$$

For larger values of x coherence effects are small, and there is in principle room for a chiral component of the partonic structure at small b and longitudinal distances $\sim 1/M_\pi$. In order to calculate this component one would need to model the finite-size effects limiting the longitudinal extension of the pion and the spectator system, which is related to the “small- x behavior” of the parton densities of the respective systems. We leave this problem to a future study. Interestingly, this could result in partial “readmission” of the small- b component of the pion cloud model which was excluded in the present study, potentially affecting *e.g.* the comparison with the measured flavor asymmetry $\bar{d} - \bar{u}$ in Sec. IV A.

We note that the interference effects in scattering from πB configurations described here are large in the region in which chiral corrections to the structure of the pion would become important, *cf.* the discussion in Sec. VII B. An interesting question is whether in the chiral perturbation theory approach these effects come into play already at the level of the leading logarithmic approximation [31], or only at the level of subleading or finite terms.

VIII. SUMMARY AND OUTLOOK

The transverse coordinate representation based on GPDs represents a most useful framework for studying the role of chiral dynamics in the nucleon's partonic structure. It allows one to identify the parametric region of the chiral component ($x \lesssim M_\pi/M_N, b \sim 1/M_\pi$) and provides a practical scheme for calculating it in a model-independent way. Let us briefly summarize the main results of our investigation.

- (a) The contributions from πB ($B = N, \Delta$) configurations to the parton distributions become independent of the $\pi N B$ form factors at transverse distances $b \gtrsim 0.5$ fm, and thus can be associated with universal chiral dynamics. The lower limit in b approximately coincides with the nucleon's core radius, $R_{\text{core}} = 0.55$ fm, inferred previously from other phenomenological considerations.
- (b) Only $\sim 1/3$ of the measured antiquark flavor asymmetry $[\bar{d} - \bar{u}](x)$ at $x > 10^{-2}$ comes from the large-distance region $b > R_{\text{core}}$, showing that most of

it resides in the nucleon's core at small transverse distances. The traditional pion cloud model, which attempts to explain the entire asymmetry from pionic contributions, gets most of the effect from small b where the concept of πB configurations is not applicable.

- (c) The isoscalar antiquark distribution $[\bar{u} + \bar{d}](x)$ obtained from pions at large b remains safely below the total antiquark distribution determined by QCD fits to deep-inelastic scattering data, leaving room for the (non-perturbatively and perturbatively generated) antiquarks in the core. This naturally solves a problem of the traditional pion cloud model, where the pionic contribution can saturate or even exceed the total antiquark density for certain non-exceptional parameter values.
- (d) The strange sea quark distributions, $s(x)$ and $\bar{s}(x)$, overwhelmingly sit at small transverse distances, $b < R_{\text{core}}$. Neither chiral ($\pi N, \pi \Delta$) nor $K\Lambda$ configurations at large b account for more than a few percent of the empirical $s + \bar{s}$. The predictions of Ref. [38] for the x -dependence of $s(x)$ and $\bar{s}(x)$ from $K\Lambda$ fluctuations rely on the region where the concept of distinct meson-baryon configurations is not applicable and require a probability of $K\Lambda$ fluctuations several times larger than what is obtained from the standard $SU(3)$ couplings.
- (e) The pionic contributions to the nucleon's transverse size, $\langle b^2 \rangle$, are much less sensitive to short-distance dynamics than those to the parton distributions themselves, and thus furnish a new set of clean chiral observables. The large-distance contributions to the nucleon's singlet quark size at $x < 0.1$ are larger than those to the gluonic size, suggesting that $\langle b^2 \rangle_{q+\bar{q}} > \langle b^2 \rangle_g$, in agreement with the pattern of t -slopes of deeply-virtual Compton scattering and exclusive J/ψ production measured at HERA and FNAL.

In the present study we have limited ourselves to the universal large-distance contributions to the partonic structure, which are governed by soft pion exchange and can be calculated in a model-independent way. A complete description should include also a model of the short-distance part, which actually carries most of the parton densities. One way of combining the two would be a two-component picture, in which the constituents in the “core” act as a source of the chiral pion fields which propagate out to distances $\sim 1/M_\pi$. Such an approach would be very effective if the characteristic transverse sizes of the “cloud” and the “core” were numerically very different. However, this is not the case — the characteristic range of two-pion exchange $1/(2M_\pi) = 0.71$ fm is numerically not much larger than our estimate of the “core” size, $R_{\text{core}} = 0.55$ fm. Another approach, which appears more promising, is based on the idea of a smooth “interpolation” between the chiral large-distance dynamics

and the short-distance regime. In particular, the effective theory of Ref. [57], which is based on the large- N_c limit of QCD, uses constituent quarks as interpolating degrees of freedom; it is valid in a wide region, from distances of the order $\sim 1/M_\pi$ down to distances of the order $\rho \approx 0.3 \text{ fm}$ — the range of the non-perturbative chiral-symmetry breaking forces in the QCD vacuum. It leads to a picture of the nucleon as quarks bound by a self-consistent pion field (chiral quark-soliton model) [58], which is fully field-theoretical and relativistic and provides a very good description of the nucleon's quark and antiquark densities, including subtle effects such as the sea quark flavor asymmetry and its polarization [54]. The results of Ref. [14] and the present work (see in particular Sec. VI) show that this large- N_c description of nucleon structure is equivalent to phenomenological soft-pion exchange at large transverse distances, thanks to the universality of chiral dynamics; it thus, in a sense, contains the result of the present work as a limiting case. Using this large- N_c picture as a script to model the impact parameter-dependent parton densities at all b , would certainly be an interesting problem for further study.

Direct experimental study of the chiral component of the nucleon's partonic structure through hard exclusive processes at $x < 0.1$ would be possible with a future electron-ion collider (EIC). The simplest observables are the t -dependences of the differential cross sections for various channels ($J/\psi, \phi, \rho, \pi$) at $|t| \ll 0.1 \text{ GeV}^2$, and their change with x ; at sufficiently large Q^2 such measurements can be related directly to the t -dependence of the gluon and quark GPDs at small t . In particular, such measurements should be able to resolve variations of the t -slope with t and possible deviations from exponential t -dependence. Measurements of exclusive processes require high luminosity and the capability to detect the recoiling baryon at small angles, which is possible with appropriate forward detectors. Another interesting option are pion knockout processes, corresponding to exclusive scattering from a pion at transverse distances $b \sim 1/M_\pi$, where both the recoiling pion and the nucleon are identified in the final state; see Ref. [14] for a detailed discussion.

The partonic content of the nucleon's pion cloud can in principle also be probed in high-energy pp collisions with

hard processes, such as dijet and Drell-Yan pair production. Such processes, including accompanying spectator interactions, are most naturally described in the transverse coordinate (impact parameter) representation employed in our investigation here. Interesting new effects appear in collisions at multi-TeV energies (LHC), where the cross sections for hard processes can approach the geometric limit (black-disk regime) and the probability for multiple hard interactions becomes significant. In this situation it is important to realize that the πB configurations participate in the high-energy scattering process with a fixed transverse orientation, which is frozen during the collision; depending on this orientation one may either have a violent collision of the pion with the other proton or no interaction at all. The averaging over the orientations of the πB configuration must be performed in the colliding pp system with given transverse geometry, not in the partonic wave functions of the individual protons. This circumstance affects *e.g.* the rate of multi-jet events in peripheral collisions [59]. More generally, the pion cloud represents an example of transverse correlations in the nucleon's partonic wave function, which are neglected in the usual mean-field approximation for high-energy pp collisions. In particular, such correlations play a role in central inclusive diffraction, where they reduce the rapidity gap survival probability relative to the mean-field result [60].

Acknowledgments

The authors are indebted to A. Freund, J. Goity, V. Guzey, N. Kivel, P. Nadolsky, M. V. Polyakov, and A. W. Thomas for enlightening discussions and useful hints.

Notice: Authored by Jefferson Science Associates, LLC under U.S. DOE Contract No. DE-AC05-06OR23177. The U.S. Government retains a non-exclusive, paid-up, irrevocable, world-wide license to publish or reproduce this manuscript for U.S. Government purposes. Supported by other DOE contracts.

-
- [1] P. Amaudruz *et al.* [New Muon Collaboration], Phys. Rev. Lett. **66**, 2712 (1991). M. Arneodo *et al.* [New Muon Collaboration], Phys. Rev. D **50**, 1 (1994).
 - [2] K. Ackerstaff *et al.* [HERMES Collaboration], Phys. Rev. Lett. **81**, 5519 (1998).
 - [3] A. Baldit *et al.* [NA51 Collaboration], Phys. Lett. B **332**, 244 (1994).
 - [4] E. A. Hawker *et al.* [FNAL E866/NuSea Collaboration], Phys. Rev. Lett. **80**, 3715 (1998).
 - [5] R. S. Towell *et al.* [FNAL E866/NuSea Collaboration], Phys. Rev. D **64**, 052002 (2001).
 - [6] S. Kumano, Phys. Rept. **303**, 183 (1998). G. T. Garvey and J. C. Peng, Prog. Part. Nucl. Phys. **47**, 203 (2001).
 - [7] A. W. Thomas, Phys. Lett. B **126**, 97 (1983).
 - [8] L. L. Frankfurt, L. Mankiewicz, and M. I. Strikman, Z. Phys. A **334**, 343 (1989);
 - [9] R. Machleidt, K. Holinde and C. Elster, Phys. Rept. **149**, 1 (1987).
 - [10] W. Koepf, L. L. Frankfurt and M. Strikman, Phys. Rev. D **53**, 2586 (1996).
 - [11] J. D. Sullivan, Phys. Rev. D **5**, 1732 (1972).
 - [12] M. Burkardt, Int. J. Mod. Phys. A **18**, 173 (2003).
 - [13] P. V. Pobylitsa, Phys. Rev. D **66**, 094002 (2002).
 - [14] M. Strikman and C. Weiss, Phys. Rev. D **69**, 054012

- (2004).
- [15] A. Aktas *et al.* [H1 Collaboration], *Eur. Phys. J. C* **46**, 585 (2006).
 - [16] S. Chekanov *et al.* [ZEUS Collaboration], *Nucl. Phys. B* **695**, 3 (2004).
 - [17] M. Binkley *et al.*, *Phys. Rev. Lett.* **48**, 73 (1982).
 - [18] M. Strikman and C. Weiss, in: Proceedings of LIGHT CONE 2008 “Relativistic Nuclear and Particle Physics,” Mulhouse, France, July 7–11, 2008; arXiv:0811.3631 [hep-ph].
 - [19] F. D. Aaron *et al.* [H1 Collaboration], *Phys. Lett. B* **659**, 796 (2008).
 - [20] S. Chekanov *et al.* [ZEUS Collaboration], arXiv:0812.2517 [hep-ex].
 - [21] M. Goncharov *et al.* [NuTeV Collaboration], *Phys. Rev. D* **64**, 112006 (2001).
 - [22] D. Mason *et al.*, *Phys. Rev. Lett.* **99**, 192001 (2007).
 - [23] J. W. Chen and X. D. Ji, *Phys. Lett. B* **523**, 107 (2001); *Phys. Rev. Lett.* **87**, 152002 (2001) [Erratum-ibid. **88**, 249901 (2002)].
 - [24] D. Arndt and M. J. Savage, *Nucl. Phys. A* **697**, 429 (2002).
 - [25] W. Detmold, W. Melnitchouk, J. W. Negele, D. B. Renner and A. W. Thomas, *Phys. Rev. Lett.* **87**, 172001 (2001).
 - [26] A. V. Belitsky and X. Ji, *Phys. Lett. B* **538**, 289 (2002).
 - [27] S. I. Ando, J. W. Chen and C. W. Kao, *Phys. Rev. D* **74**, 094013 (2006).
 - [28] M. Diehl, A. Manashov and A. Schafer, *Eur. Phys. J. A* **29**, 315 (2006). *Eur. Phys. J. A* **31**, 335 (2007).
 - [29] N. Kivel and M. V. Polyakov, arXiv:hep-ph/0203264. *Phys. Lett. B* **664**, 64 (2008).
 - [30] R. D. Young, D. B. Leinweber and A. W. Thomas, *Nucl. Phys. Proc. Suppl.* **141**, 233 (2005).
 - [31] N. Kivel, M. V. Polyakov and A. Vladimirov, *Phys. Rev. D* **79**, 014028 (2009); *Phys. Rev. Lett.* **101**, 262001 (2008).
 - [32] L. Frankfurt and M. Strikman, *Phys. Rev. D* **66**, 031502 (2002).
 - [33] V. R. Zoller, *Z. Phys. C* **53**, 443 (1992).
 - [34] W. Melnitchouk and A. W. Thomas, *Phys. Rev. D* **47**, 3794 (1993).
 - [35] W. Melnitchouk, J. Speth and A. W. Thomas, *Phys. Rev. D* **59**, 014033 (1999).
 - [36] M. Gluck, E. Reya and I. Schienbein, *Eur. Phys. J. C* **10**, 313 (1999).
 - [37] A. D. Martin, W. J. Stirling, R. S. Thorne and G. Watt, arXiv:0901.0002 [hep-ph].
 - [38] S. J. Brodsky and B. Q. Ma, *Phys. Lett. B* **381**, 317 (1996).
 - [39] M. Gluck, P. Jimenez-Delgado and E. Reya, *Eur. Phys. J. C* **53**, 355 (2008).
 - [40] H. L. Lai, P. M. Nadolsky, J. Pumplin, D. Stump, W. K. Tung and C. P. Yuan, *JHEP* **0704**, 089 (2007).
 - [41] H. Holtmann, A. Szczurek and J. Speth, *Nucl. Phys. A* **596**, 631 (1996).
 - [42] L. Frankfurt, M. Strikman and C. Weiss, *Phys. Rev. D* **69**, 114010 (2004).
 - [43] K. Goeke, M. V. Polyakov and M. Vanderhaeghen, *Prog. Part. Nucl. Phys.* **47**, 401 (2001). M. Diehl, *Phys. Rept.* **388**, 41 (2003). A. V. Belitsky and A. V. Radyushkin, *Phys. Rept.* **418**, 1 (2005).
 - [44] L. Frankfurt, A. Freund, V. Guzey and M. Strikman, *Phys. Lett. B* **418**, 345 (1998) [Erratum-ibid. **B 429**, 414 (1998)].
 - [45] A. G. Shuvaev, K. J. Golec-Biernat, A. D. Martin and M. G. Ryskin, *Phys. Rev. D* **60**, 014015 (1999).
 - [46] A. Levy, arXiv:0905.2034 [hep-ex].
 - [47] M. Strikman and C. Weiss, in: Proceedings of the workshop: HERA and the LHC workshop series on the implications of HERA for LHC physics, Eds. H. Jung *et al.*, arXiv:0903.3861 [hep-ph].
 - [48] A. Freund and M. F. McDermott, *Phys. Rev. D* **65**, 091901 (2002).
 - [49] H. Lim, L. Schoeffel and M. Strikman, in: “Summary of the ‘Diffraction and vector mesons’ working group at DIS06,” Proceedings of 14th International Workshop on Deep Inelastic Scattering (DIS 2006), Tsukuba, Japan, 20–24 Apr 2006, pp. 853–866; arXiv:hep-ph/0608107.
 - [50] S. A. Morrow *et al.* [CLAS Collaboration], *Eur. Phys. J. A* **39**, 5 (2009).
 - [51] M. Guidal, M. V. Polyakov, A. V. Radyushkin and M. Vanderhaeghen, *Phys. Rev. D* **72**, 054013 (2005).
 - [52] M. Diehl, T. Feldmann, R. Jakob and P. Kroll, *Eur. Phys. J. C* **39**, 1 (2005).
 - [53] M. Gluck, E. Reya and A. Vogt, *Eur. Phys. J. C* **5**, 461 (1998).
 - [54] D. Diakonov, V. Petrov, P. Pobylitsa, M. V. Polyakov and C. Weiss, *Nucl. Phys. B* **480**, 341 (1996); *Phys. Rev. D* **56**, 4069 (1997).
 - [55] G. S. Adkins, C. R. Nappi and E. Witten, *Nucl. Phys. B* **228**, 552 (1983).
 - [56] L. L. Frankfurt and M. I. Strikman, *Phys. Rept.* **76**, 215 (1981).
 - [57] D. Diakonov and M. I. Eides, *JETP Lett.* **38**, 433 (1983) [*Pisma Zh. Eksp. Teor. Fiz.* **38**, 358 (1983)]. D. Diakonov and V. Y. Petrov, *Nucl. Phys. B* **272**, 457 (1986).
 - [58] D. Diakonov, V. Y. Petrov and P. V. Pobylitsa, *Nucl. Phys. B* **306**, 809 (1988).
 - [59] T. C. Rogers, A. M. Stasto and M. I. Strikman, *Phys. Rev. D* **77**, 114009 (2008).
 - [60] L. Frankfurt, C. E. Hyde, M. Strikman and C. Weiss, *Phys. Rev. D* **75**, 054009 (2007).
 - [61] V. Guzey and M. V. Polyakov, arXiv:hep-ph/0512355.
 - [62] The approach taken here bears some similarity to the use of finite-size regulators in the chiral extrapolation of lattice QCD results [30].
 - [63] In invariant perturbation theory soft pions have virtualities $-k_\pi^2 \sim M_\pi^2$, and Eq. (1) results from the condition that the minimum pion virtuality which is kinematically required for a given longitudinal momentum fraction, y , be at most of the order M_π^2 ; cf. Eq. (13) below.
 - [64] The relation between the distance of a constituent from the transverse center-of-momentum, b , and its distance from the center-of-momentum of the spectator system, r , can easily be derived for the case of a non-interacting system, by starting from the well-known expression for the center-of-mass in the rest frame and performing a boost to large velocity, taking into account that for the non-interacting system the longitudinal momentum fractions are given by the ratios of the constituent masses to the total mass of the system. A more formal derivation, based on the light-cone components of the energy-momentum tensor, can be found in Ref. [12].
 - [65] In Ref. [14] the pion virtualities were denoted by $-s_\pm$. Here we denote them by $t_{1,2}$, reserving $s_{1,2}$ for the invariant masses of the πB system, Eq. (20).
 - [66] Equation (46) of Ref. [14] incorrectly writes the convo-

lution formula for the antiquark flavor asymmetry with the antiquark density in the pion rather than the valence quark density. The correct expression is with the valence quark density, *cf.* Eq. (28). This does not affect the conclusions about the large- N_c behavior presented in Ref. [14], which was the sole point of the discussion there.

- [67] The relation of our conventions for the pion parton densities to those of Ref. [36] (GRS) is $q_\pi^{\text{val}} = \frac{1}{2}v_\pi(\text{GRS})$, $q_\pi^{\text{sea}} = \bar{q}_\pi(\text{GRS})$.
 [68] The value quoted here corresponds to the arithmetic mean of the parametrizations of $\alpha'_{J/\psi}$ quoted by the HERA H1 [15] and ZEUS [16] experiments; see Ref. [47] for details.

APPENDIX A: MESON-BARYON COUPLINGS FROM $SU(3)$ SYMMETRY

In this appendix we summarize the meson-baryon couplings used in the calculation of $SU(3)$ octet meson (π, K, η) contributions to the sea quark distributions (see Sec. IV C) and derive the expressions for the corresponding meson momentum distributions in the nucleon.

For the coupling constants governing the $N \leftrightarrow M + B$ transitions we rely on $SU(3)$ flavor symmetry, which is known to describe the empirical couplings well; see Ref. [61] for a recent review. For $\mathbf{8} \leftrightarrow \mathbf{8} \times \mathbf{8}$ transitions there are two independent $SU(3)$ -invariant structures, with coupling constants traditionally denoted by F and D . With the standard assignments of the meson and baryon fields the Lagrangian takes the form (we show explicitly only the terms describing transitions $M + B \rightarrow p$)

$$\begin{aligned} \mathcal{L} = & g_8 \bar{p} \left[\pi^+ n + \frac{1}{\sqrt{2}} \pi^0 p - \frac{1}{\sqrt{6}} (1 + 2\alpha) K^+ \Lambda \right. \\ & + (1 - 2\alpha) \left(\frac{1}{\sqrt{2}} K^+ \Sigma^0 + K^0 \Sigma^+ \right) \\ & \left. - \frac{1}{\sqrt{6}} (1 - 4\alpha) \eta p \right] + \text{h.c.} \end{aligned} \quad (\text{A1})$$

Here $g_8 \equiv F + D$ is the overall octet coupling, which is related to our πNN coupling as

$$g_{\pi NN} \equiv g_{\pi^0 pp} = g_8 / \sqrt{2}; \quad (\text{A2})$$

we use $g_{\pi NN} = 13.05$ in our numerical calculations [10]. The ratio $\alpha \equiv F/(F + D)$ remains a free parameter in the context of $SU(3)$ flavor symmetry and can only be determined empirically or by invoking dynamical models. The $SU(6)$ spin-flavor symmetry of the non-relativistic quark model implies $F/D = 2/3$, and thus

$$\alpha = 2/5 = 0.4; \quad (\text{A3})$$

we use this value in our numerical studies in Sec. IV C.

For $\mathbf{8} \leftrightarrow \mathbf{8} \times \mathbf{10}$ transitions there is only a single $SU(3)$ -invariant structure, and the Lagrangian is of the form

$$\begin{aligned} \mathcal{L} = & g_{10} \bar{p} \left(\frac{1}{\sqrt{3}} \pi^+ \Delta^0 + \sqrt{\frac{2}{3}} \pi^0 \Delta^+ - \pi^- \Delta^{++} \right. \\ & \left. + \frac{1}{\sqrt{6}} K^+ \Sigma^{*0} - \frac{1}{\sqrt{3}} K^0 \Sigma^{*+} \right) + \text{h.c.} \end{aligned} \quad (\text{A4})$$

The decuplet coupling g_{10} coincides (up to the sign) with our $\pi N \Delta$ coupling,

$$g_{\pi N \Delta} \equiv g_{\pi^- p \Delta^{++}} = -g_{10}; \quad (\text{A5})$$

we use $g_{\pi N \Delta} = 20.22$, which is close to the large- N_c value of $(3/2) g_{\pi NN}$, *cf.* Eq. (69). Note that our definition of the coupling constant $g_{\pi N \Delta}$ differs from the one of Ref. [10] by a factor, $g_{\pi N \Delta}(\text{Ref. [10]}) = \sqrt{2} g_{\pi N \Delta}(\text{this work})$.

The GPDs of $SU(3)$ octet meson in the nucleon, $H_{MB}(y, t)$, and the corresponding impact parameter-dependent distributions are obtained by straightforward

extension of the expressions for πN and $\pi\Delta$ in Sec. II, cf. Eqs. (14) and (15), and Eqs. (16)–(18). We work with the isoscalar distributions, in which we sum over the isospin components of the intermediate meson–baryon system. Using the couplings provided by Eqs. (A1) and (A4), they are obtained as (we omit the arguments for brevity)

$$\begin{aligned}
H_{\pi N} &\equiv H_{\pi^+n} + H_{\pi^0p} &= 3 g_{\pi NN}^2 I_8, \\
H_{\eta N} &\equiv H_{\eta p} &= \frac{1}{3} g_{\pi NN}^2 (1 - 4\alpha)^2 I_8, \\
H_{K\Lambda} &\equiv H_{K^+\Lambda} &= \frac{1}{3} g_{\pi NN}^2 (1 + 2\alpha)^2 I_8, \\
H_{K\Sigma} &\equiv H_{K^+\Sigma^0} + H_{K^0\Sigma^+} &= 3 g_{\pi NN}^2 (1 - 2\alpha)^2 I_8, \\
H_{\pi\Delta} &\equiv H_{\pi^+\Delta^0} + H_{\pi^0\Delta^+} \\
&\quad + H_{\pi^-\Delta^{++}} &= 2 g_{\pi N\Delta}^2 I_{10}, \\
H_{K\Sigma^*} &\equiv H_{K^+\Sigma^{*0}} + H_{K^0\Sigma^{*+}} &= \frac{1}{3} g_{\pi N\Delta}^2 I_{10}.
\end{aligned} \tag{A6}$$

Here I_8 and I_{10} are the basic momentum integrals of Eqs. (16)–(18), taken at the appropriate values of the meson and baryon masses. Note that because of isospin symmetry the distributions for the individual isospin components are all proportional to the same function and can be expressed in terms of the isoscalar distribution as

$$H_{\pi^+n} = \frac{2}{3} H_{\pi N}, \quad H_{\pi^0p} = \frac{1}{3} H_{\pi N}, \quad \text{etc.} \tag{A7}$$

where the proportions are determined by the squares of the coupling constants in the Lagrangian. The corresponding b -dependent distributions, $f_{MB}(y, b)$, are then obtained by substituting these GPDs in Eq. (8).

To determine the coefficients with which the different mesons contribute to a given parton density in the proton, one must account for the probability with which the parton occurs in the individual meson charge states. For example (in abbreviated notation)

$$\begin{aligned}
(\bar{d} - \bar{u})_p &= f_{\pi^+n}(\bar{d} - \bar{u})_{\pi^+} + f_{\pi^0p}(\bar{d} - \bar{u})_{\pi^0} \\
&= \frac{2}{3} f_{\pi N} q_{\pi^+}^{\text{val}},
\end{aligned} \tag{A8}$$

where $q_{\pi^+}^{\text{val}}$ denotes the valence quark distribution in the pion, Eq. (31), and we have used Eq. (A7) for the impact parameter distribution and the isospin and charge conjugation relations for the parton densities in the pion, $\bar{u}_{\pi^+} = d_{\pi^+}$, $\bar{u}_{\pi^0} = \bar{d}_{\pi^0}$.

APPENDIX B: EVALUATION OF COORDINATE-SPACE DISTRIBUTIONS

In this appendix we present expressions suitable for numerical evaluation of the transverse coordinate-dependent distribution of pions in the nucleon and their partial radial integrals. The b -dependent distribution, defined by Eq. (8), is evaluated as (we omit the argument y and the subscript for brevity)

$$f(b) = \int \frac{d^2\Delta_\perp}{(2\pi)^2} e^{-i(\Delta_\perp \cdot b)} H(t) \tag{B1}$$

$$= \frac{1}{2\pi} \int_0^\infty d\Delta_\perp \Delta_\perp J_0(\Delta_\perp b) H(t) \tag{B2}$$

where $b = |b|$, $\Delta_\perp = |\Delta_\perp|$, $t = -\Delta_\perp^2$, and J_0 denotes the Bessel function. Equation (B2) can be used to calculate the $f(b)$ corresponding to a numerically given $H(t)$, as obtained from evaluating the loop integral Eq. (16) with πN form factors. In practice, since $H(t)$ shows only a power-like fall-off at large $-t > 0$, we multiply the integrand in Eq. (B2) by an exponential convergence factor, $\exp(\epsilon t)$, calculate the integral numerically for finite ϵ , and estimate the limiting value for $\epsilon \rightarrow 0$ from the numerical data at finite ϵ .

From Eq. (B2) we can also derive expressions for the partial radial integrals of $f(b)$, including those with a weighting factor b^2 . Using standard identities for integrals of the Bessel function multiplied by powers of its argument, we obtain for the integrals over the region $b < b_0$

$$\int d^2b \Theta(b < b_0) f(b) = b_0 \int_0^\infty d\Delta_\perp J_1(z_0) H(t) \tag{B3}$$

$$\begin{aligned}
\int d^2b \Theta(b < b_0) f(b) b^2 &= b_0^2 \int_0^\infty \frac{d\Delta_\perp}{\Delta_\perp} [2J_0(z_0) \\
&\quad + (z_0 - 4/z_0) J_1(z_0)] H(t),
\end{aligned} \tag{B4}$$

where

$$z_0 \equiv \Delta_\perp b_0. \tag{B5}$$

The complementary integrals over the region $b > b_0$ are calculated by re-writing the original Fourier integral for $f(b)$, Eq. (B1), in the form

$$\int d^2b \Theta(b > b_0) f(b) = \int d^2b - \int d^2b \Theta(b < b_0). \tag{B6}$$

The unrestricted integral on the R.H.S. then produces a two-dimensional delta function at $\Delta_\perp = 0$ and can be evaluated in terms of $H(t = 0)$ or its derivative. In this way we obtain

$$\begin{aligned}
&\int d^2b \Theta(b > b_0) f(b) \\
&= H(t = 0) - \int d^2b \Theta(b < b_0) f(b),
\end{aligned} \tag{B7}$$

$$\begin{aligned}
&\int d^2b \Theta(b > b_0) b^2 f(b) \\
&= 4 \frac{\partial H}{\partial t}(t = 0) - \int d^2b \Theta(b < b_0) b^2 f(b),
\end{aligned} \tag{B8}$$

where the right-hand side can be evaluated using Eqs. (B3) and (B4). Note that the Δ_\perp integrals representing the b -integrated distributions, Eqs. (B3) and (B4), converge more rapidly at large Δ_\perp than the integral representing the original $f(b)$, Eq. (B2), and can therefore more easily be computed numerically.